

## Chapter

# Generation of Mud Volcanic Systems Sourced in Dehydrated Serpentspheric Mantle: A ‘Deep-to-Seep’ Model for the Zechstein Salines-Kupferschiefer Cu-Ag Deposits

*Stanley B. Keith, Jan C. Rasmussen and Volker Spieth*

## Abstract

Mud volcanism can provide a mechanism for hot hydrothermal muds and brines to ascend from dehydrated, serpentinitized peridotite at the mantle-crust contact (Moho). Such mud volcanism may have occurred on a regional scale across northern Europe when high to low density brines erupted as metalliferous, hot, hydrothermal, hydrocarbon-rich mud slurries. These mud-brines were delivered to the Permo-Triassic unconformity in a shallow Zechstein sea during the Pangea breakup through a series of deep-seated conduits that connected the serpentosphere to the Zechstein unconformity. A three-stage, hot, hydrothermal, mud volcanic model can explain the Kupferschiefer-Zechstein-Rote Fäule sequence of polymetallic, hydrocarbon, and saline mineralization as a consequence of a three-stage, dehydration sequence of deep serpentospheric uppermost mantle. Dehydration products of mantle-heated serpentinite were produced in three sequential stages: (1) lizardite to antigorite, (2) antigorite to chlorite-harzburgite, and (3) chlorite-harzburgite to garnet peridotite. The dehydration of serpentine correlates to three stages of Zechstein-Kupferschiefer mineralization: (1) Weissliegend-Kupferschiefer Cu-Ag-carbonaceous shale and silica sand deposits, to (2) Zechstein saline deposits, to (3) Rote Fäule hematite-Au-REE-U cross-cutting metallization.

**Keywords:** mud volcanism, brines, Zechstein, Kupferschiefer, saline deposits, copper silver deposits, serpentosphere, serpentinite, peridotite, lizardite, antigorite, hydrocarbon

## 1. Introduction

The Kupferschiefer is a copper-, polymetallic-, hydrocarbon-bearing black shale of the lowermost Zechstein Group of Permo-Triassic age (252 Ma) in southern Germany and southwestern Poland [1, 2]. It is usually one to two-meters thick and

underlies 600,000 square kilometers, extending from Great Britain to Belarus for a distance of over 1500 km (**Figure 1**).

Copper has been mined from the Kupferschiefer for over 800 years, since its discovery circa 1200 A.D. The top of the Kupferschiefer carbonaceous shale unit coincides with the Permian extinction event and the Permo-Triassic unconformity dated at circa 252 Ma [1, 2]. The brines that deposited the Kupferschiefer metal system were extremely toxic and reduced and may have significantly contributed to the Permian extinction event [3].

Mineralogical, chemical, and geological analyses of the combined Kupferschiefer-Zechstein show strong chemical and paragenetic relationships between the Weissliegend silica extrudites (sandstones), Kupferschiefer carbonaceous shales, and Zechstein salines and dolomitic carbonates. This linkage has led us to a broader, more unified, serpentine-linked model related to deep-sourced, hot, hydrothermal, mud-brine volcanism [1, 2]. The overall Zechstein-Kupferschiefer chemical stratigraphy suggests density- and composition-driven fractionation of deep-sourced, high-density brines that are metal-rich, alkali-rich, silica-aluminum-rich, and halogen-rich.

The Kupferschiefer-Weissliegend contains a world-class copper resource with most of the copper hosted in the Weissliegend. More than 78 million metric tons (Mt) of copper have been produced or delineated as resources, with more than 90 percent of the known mineral endowment located in Poland [4]. Salt resources in the immediately overlying Zechstein saline sequence are also world-class with 102 billion metric tons of economic and subeconomic salt in Poland alone [5]. The salt deposits also contain major resources of magnesium and potassium along with elevated strontium, boron, and lithium [6].

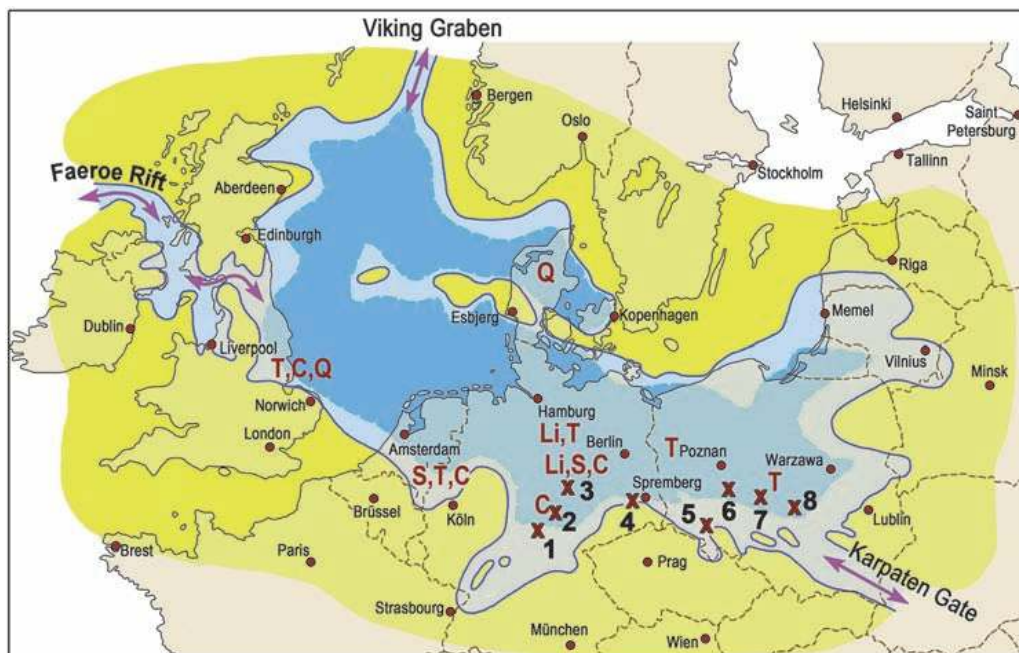


**Figure 1.**

Map of Zechstein basin showing locations of exotic magnesium minerals, lithium-rich brines, and euhedral quartz [1]. [Li = lithium-rich brines; T = talc; S = serpentine; C = clinocllore; Q = euhedral quartz]. From west to east (left to right), the locations are Yorkshire, England [TCQ], Emsland, southwest Germany [STC], Mors diapir, northern Denmark [Q], Gorleben salt dome north central Germany [Li,T], Morsleben salt dome [Li,S,C], Königsschall, Hindenburg salt mine, southern Germany [C], dolomite 'reef'. Red x crosses are mines: 1 = Melsungen, 2 = Sangerhausen, 3 = Mansfeld, 4 = Spremberg, 5 = Konrad, 6 = Polkowice-Sieroszwice, 7 = Rudna, and 8 = Lubin.

## 1.1 Purpose

Three hydrothermal heat pulses were posited to represent different stages of dehydration of serpentine in the underlying ultramafic basement [1]. The current paper tests that hypothesis by examining chemical evidence in serpentinite basements for (1) general evidence for dehydration, (2) specific evidence for sequential dehydration, and (3) qualitative mass balance constraints that relate to sequential emplacement of brines in the overlying Kupferschiefer-Zechstein.

This paper also examines possible structures connecting the basement and overlying strata and to what extent a serpentinitized zone underlies Poland and Germany. Spieth [2] and Spieth and others [4] added refinements to the high-temperature aspects of the hydrothermal, mud volcanic, mud-brine model. This paper provides an expanded definition of the serpentsphere, especially those emplaced at the base of the crust during flat subduction episodes. This paper also develops a geochemical model that links sequenced dehydration of the serpentsphere with the paragenetic sequence in the overlying Kupferschiefer-Zechstein hydrothermalism and attendant mud volcanism (Figure 2).

## 1.2 Geologic setting

The general hydrothermal mud reaction sequence for the Kupferschiefer itself starts with early silica, copper-silver-gold-rich, illitic, carbonaceous (kerogen-rich) shale. The Kupferschiefer-Zechstein sequence rapidly grades upward, becoming more dolomitic up section, with a zinc-rich zone associated with dolomitic

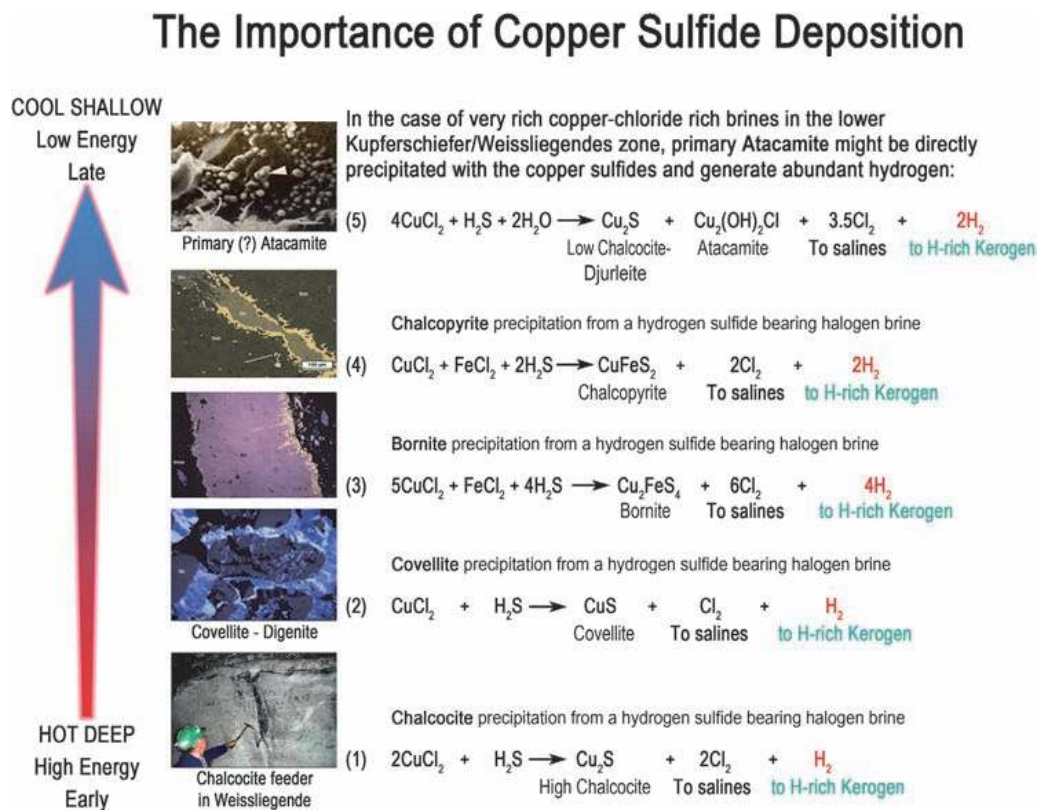


**Figure 2.**  
 Copper sulfide deposition and reaction products inferred in this paper.

carbonate, followed by calcitic carbonate. The carbonates near the base of the Zechstein transition upward into a saline-rich chemical lithocap, which comprises the multi-cyclic, Zechstein chemical sedimentary sequence. The lowest Zechstein cycle is the Werra carbonate, which grades upward into a basal, anhydrite-rich unit that transitions upward into halite. At least two additional cycles, each flooded by carbonates, in turn grade upward to halite and then into magnesium- and potassium-chlorides. The Rote Fäule represents a late stage, oxidized, hematitic alteration that post-dated the Kupferschiefer and penetrated upward at least into the basal Werra anhydrite unit of the Zechstein sequence.

### **1.3 Conceptual model**

The extensive literature on the Kupferschiefer was canvassed [1, 2] and revealed evidence for a hot, hydrothermal, mud volcanism model that was sourced in a serpentosphere layer that had earlier been tectonically emplaced by flat subduction between the crust and mantle (Moho). This paper focuses on the deep crustal sources from which the Kupferschiefer and related strata were possibly sourced. The result is a consistent, crustal-scale model of ultra-deep hydrothermalism (UDH) that is derived from ultramafic sources (serpentosphere) in the lower crust under high energy conditions.

In the mud volcano model, metal-rich brines ascended through deep-reaching faults and erupted as lower temperature slurries on low-relief, shield-shaped mud volcanoes above fractures in an open, shallow inland sea. Metal sulfide deposition is systematically accompanied by co-precipitation of silica, dolomitic carbonate, and muscovite/illite, as well as primary copper chlorides (such as atacamite [CuCl<sub>2</sub>]) and other brine minerals, such as anhydrite and sylvite [KCl]. Hydrocarbons are also an important co-precipitate [1, 2].

In the mud-volcanic model, the underlying Weissliegend Sandstone is reinterpreted to be a silica-injectite/extrudite complex that was deposited as an early silica mud fractionate of the Zechstein-Kupferschiefer, chemical, mud-brine volcanism [1, 2]. In the main Kupferschiefer copper areas, the Weissliegend contains chalcocite (with minor bornite and illite) in silica matrix. The Weissliegend and Rotliegend host significant oil and gas accumulations in nearby areas. The hydrocarbons may also have a hydrothermal origin that is related to hydrogenation of primary kerogen in the mud-brine plume.

The ultimate brine source is interpreted by Keith and others [1, 2] to be serpentinized peridotite in the lower crust near the Moho transition to the mantle. Dehydration of the serpentinite source to talc (steatization) by mantle heat during failed, intra-continental rifting of the Pangaea supercontinent at the end of Permian time is suggested to have released vast amounts of element-laden, high-density brines into deep basement fractures. The chemical muds were then deposited into and above the Rotliegend Sandstone in the shallow Kupferschiefer-Zechstein sea at the Permo-Triassic unconformity [1, 2].

The Kupferschiefer situation is analogous to modern mud volcanism in the northern Caspian Sea, the 700-km long and 50-km wide belt of mud volcanoes of the Mariana forearc wedge, and Salton Sea gryphons of southern California, USA. The UDH model of a mud volcanic origin of brines integrates the concepts of researchers favoring the hot epigenetic model with those favoring the cold syngenetic model.

Three pulses were identified in the broader Kupferschiefer-Zechstein metallization sequence through examination of the mineral paragenesis and an extensive radiometric age data set reported in a literature survey [1]. These three pulses are represented by the following (with less common constituents in parentheses):

1. Weissliegend-Kupferschiefer - Cu-Ag (Re, Pb) metallization and hydrocarbon synthesis at 265–255 Ma,
2. Zechstein - Zn-Cu-Pb-Ag metallization and continued hydrocarbon synthesis and petroleum generation at 250–245 Ma, and
3. Rote Fäule - Au-(PGE-U-Co-Se) metallization at 245–235 Ma.

## 2. Observations consistent with serpentosphere source

The hot, hydrothermal, serpentosphere-sourced, mud volcanic model integrates with several recent observations that are problematic for existing models. These observations include the following:

1. High- and low-temperature sulfides coexist. High-temperature selenides were identified by microprobe studies conducted by Spieth [2]. Low-temperature sulfide species, such as djurleite and low chalcocite, co-formed in surface or near surface eruptive sites. These low-temperature sulfides appear in the same sample as high-temperature species, such as selenides that would have formed in deeper mud chambers.
2. Alkylated and hydrogenated kerogens systematically increase up section following abundant copper sulfide deposition in the T-1 horizon.
3. The possible presence of chloride brines is evidenced by possible primary atacamite that is coeval with copper sulfide deposition in the Weissliegend (**Figure 2**).
4. High crystallinity illite (muscovite) was co-deposited with copper sulfides and has closure temperatures at circa 350°C [1].
5. Alkane oils were produced in an experiment at 350°C from Kupferschiefer black shales under hydrothermal pyrolysis conditions by Lewan and others [7, 8].

### 2.1 Density-driven mineral fractionations

Mineral paragenesis in the combined Weissliegend-Kupferschiefer-Zechstein sequence can be characterized as a density-driven fractionation process. Heavier minerals generally appear earlier and deeper in the sequence in the Kupferschiefer and lighter minerals appear later and higher in the Zechstein sequence.

The intimate association of hydrocarbon generation coinciding with sulfide deposition is shown in **Figure 3**, where a small diapiric body of zoned sulfides projects into the soft marls of the lower Zechstein at the hydrocarbon generation horizon. This relationship demonstrates the hydrogenation effect induced by sulfide deposition from chloride-rich brines, per the chemistry shown in **Figure 2**. The diapir-like shape of the sulfide mineralization can be inferred to represent a small-scale analog of the vertical pipe-like features present throughout the Kupferschiefer. The entire depositional sequence appears to be more or less coeval and occurred under soft, mud slurry conditions that were migrating upward from high pressure to low pressure.

Fractionation occurs at all scales within the Kupferschiefer section. At the broad system scale, mineral densities generally become lighter up-section and with decreasing age (**Table 1**). At the deposit scale (**Figure 4**), pipe-like features have been

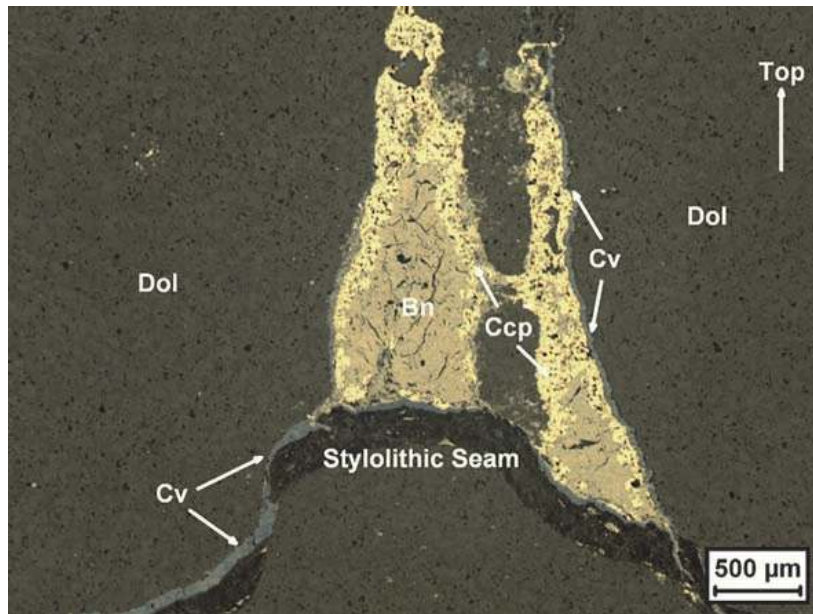


**Figure 3.** Immiscible bornite-chalcopyrite-injectite with covellite, solid state exsolution into soft, carbonaceous-dolomitic muds of the Zechstein dolostone, mounted on a stylolite of massive bitumen hydrocarbon. Spremberg DH 131. //Nic. [2].

intersected by drillholes beneath the Rudna mound. At the district scale (**Figure 5**), a, high-density, heavy, noble element suite (Au, PGE, U) is associated with the late-stage, Rote Fäule and is present near deep-seated pipes or fault conduits, such as the Odra fault, as documented by Kucha [9]. Many of Kucha's observations anticipate the perspectives offered here. Deep-seated pipe structures might be located beneath high density, uranium-rich, gamma anomalies along and near the Odra fault [9, 10].

The early, high-density, copper-rich mineral suite occurs at the base of the Kupferschiefer in the famous, high copper-grade, T-1 unit and in the more recently mined, Weissliegend basal unit of the Zechstein in the Rudna area of southwest Poland. The copper facies and kerogen mainly formed during the widespread Stage 1 episode.

After a short pause, chalcopyrite-sphalerite- and lesser galena were deposited in the basal Zechstein dolomitic marls. The lead facies and bitumen corresponds to Stage 2. Low-density hydrocarbons and calcitic marls co-formed and continued to form after the dolomitic marls along with pyritic sulfides. The final phases of Zechstein deposition were associated with a low density, saline mineral suite. Within this saline mineral suite, a density-driven zoning is apparent. Higher density anhydrite occurs in the lower cycles and lower density, magnesium-potassium halides (carnallite, kieserite, and sylvite) occur in the higher cycles. Halite deposition is widespread, but appears to be maximized in the middle cycles.

## 2.2 Carbon isotopes

Carbon isotope data for the Kupferschiefer are also consistent with other isotope data that indicate a deep serpentosphere source. The  $\delta^{13}\text{C}$  isotope data for all Kupferschiefer samples are shown in **Figure 6** and range from  $-23$  to  $-28\text{‰}$  [11–18]. The Kupferschiefer carbon isotopes completely overlap those of oceanic serpentinite seawater peridotite inclusions. Carbon isotopes from Kupferschiefer plot in the middle of the serpentinite-peridotite-kerogen oil window.

Important additional carbon isotope correlations include those for dissolved kerogen (DOC) in deep sea water, saline, hydrothermal fluids from deep marine

Compound	Formula	Density
<b>Saline lithocap</b>		
Carnallite	KMgCl <sub>3,6</sub> H <sub>2</sub> O	1.6
Sylvite	KCl	1.96
Kieserite	MgSO <sub>4</sub> ·H <sub>2</sub> O	2.6
Halite	NaCl	2.15
Anhydrite	CaSO <sub>4</sub>	2.95
<b>Kupferschiefer-Zechstein</b>		
Kerogen	HC	1.15
Carbon	C	2.3
Quartz	SiO <sub>2</sub>	2.64
Calcite	CaCO <sub>3</sub>	2.71
Muscovite	KAl <sub>2</sub> (AlSi <sub>3</sub> O <sub>10</sub> )(OH) <sub>2</sub>	2.81
Dolomite	CaMg(CO <sub>3</sub> ) <sub>2</sub>	2.88
<b>Near and away from vent</b>		
Sphalerite	ZnS	4.0
Chalcopyrite	CuFeS <sub>2</sub>	4.2
Pyrite	FeS <sub>2</sub>	4.9
Galena	PbS	7.57
<b>Near and on vent</b>		
Covellite	CuS	4.61
Bornite	Cu <sub>5</sub> FeS <sub>4</sub>	5.075
Hematite	Fe <sub>2</sub> O <sub>3</sub>	5.26
Digenite	Cu <sub>9</sub> S <sub>5</sub>	5.55
Chalcocite	Cu <sub>2</sub> S	5.8
<b>On and in (?) vent</b>		
Palladoarsenide	Pd <sub>2</sub> As	10.4
Silver	Ag	10.5
Sperrylite	PtAs <sub>2</sub>	10.6

**Table 1.**  
*Paragenetic sequence and zoning integrated with mineral densities for the Kupferschiefer-Zechstein section (youngest at top).*

seeps hosted in basalt on the Juan de Fuca Ridge, and a partial overlap with serpentine-sourced hydrothermal fluids emanating from white smokers at Lost City in the central Atlantic Ocean. There is also a complete overlap with carbon isotopes in world-wide oil. This carbon isotope correlation allows the inference that the serpentsphere described below is the ultimate source of oil, carbonaceous shale, and metallization in the Kupferschiefer.

### 2.3 Sulfur isotopes

An isotopic feature that is unique to the Kupferschiefer-Zechstein sulfide system is the extremely light sulfur isotope data at Lubin (**Figure 7**) [19]. In chalcocite-digenite samples, the  $\delta^{32}\text{S}$  reaches values as low as  $-39.9\%$ . Pyrite samples are

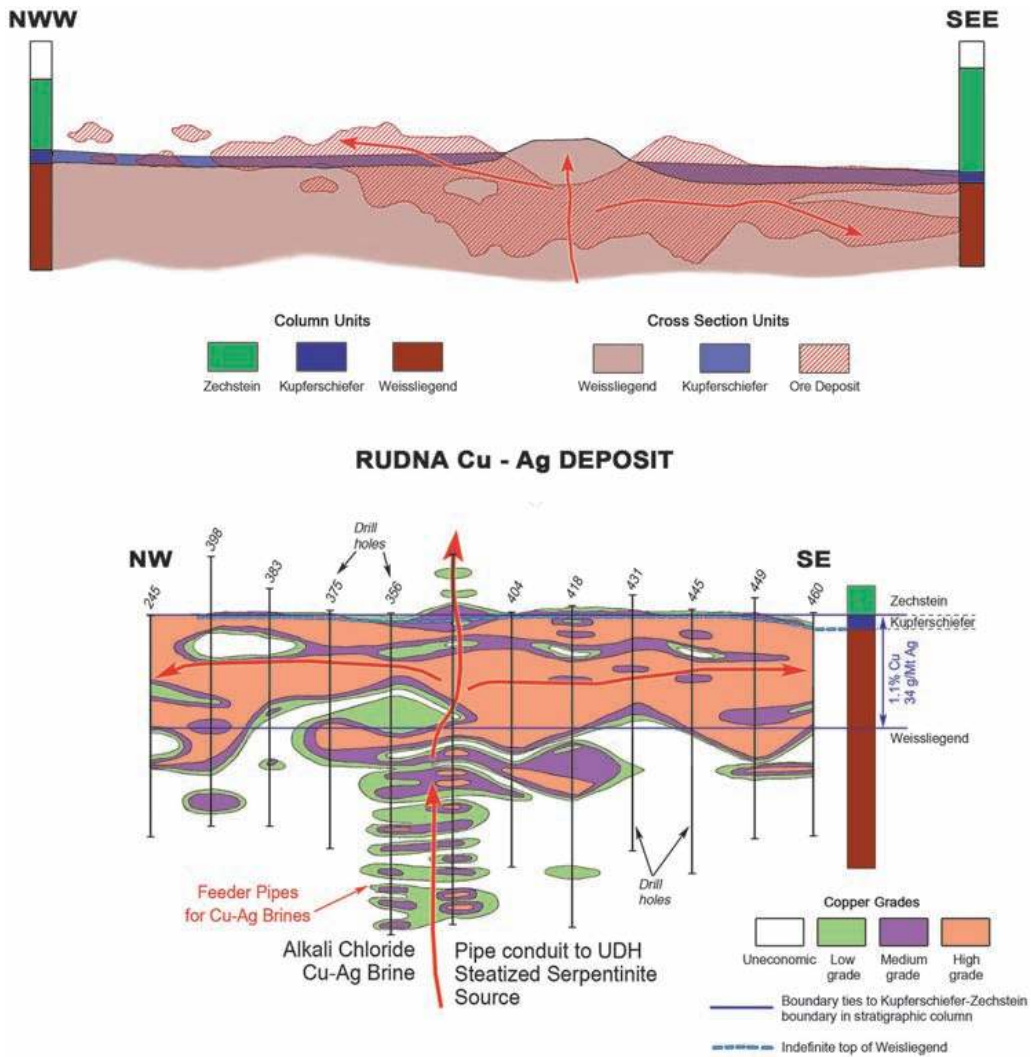


**Figure 4.** Deposit-scale cross section of the Rudna deposit showing that smaller-scale pipe structures are also present at larger scales (modified from [11]).

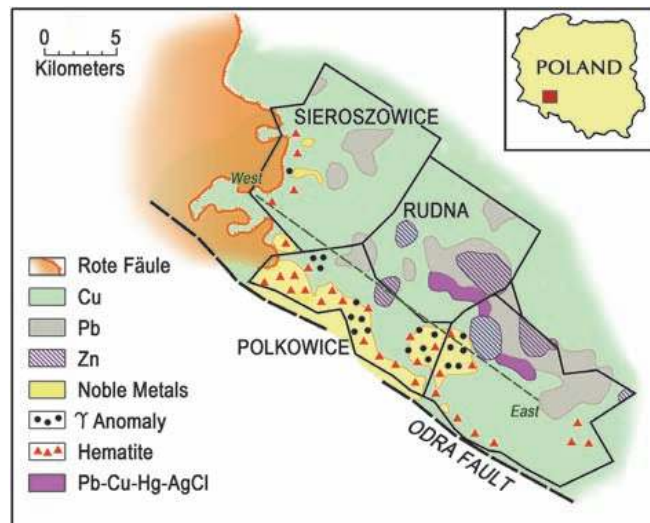


**Figure 5.** Regional metal zoning in the greater Lubin district and its geographic relationship to the deep-seated Odra fault (adapted from [9]).



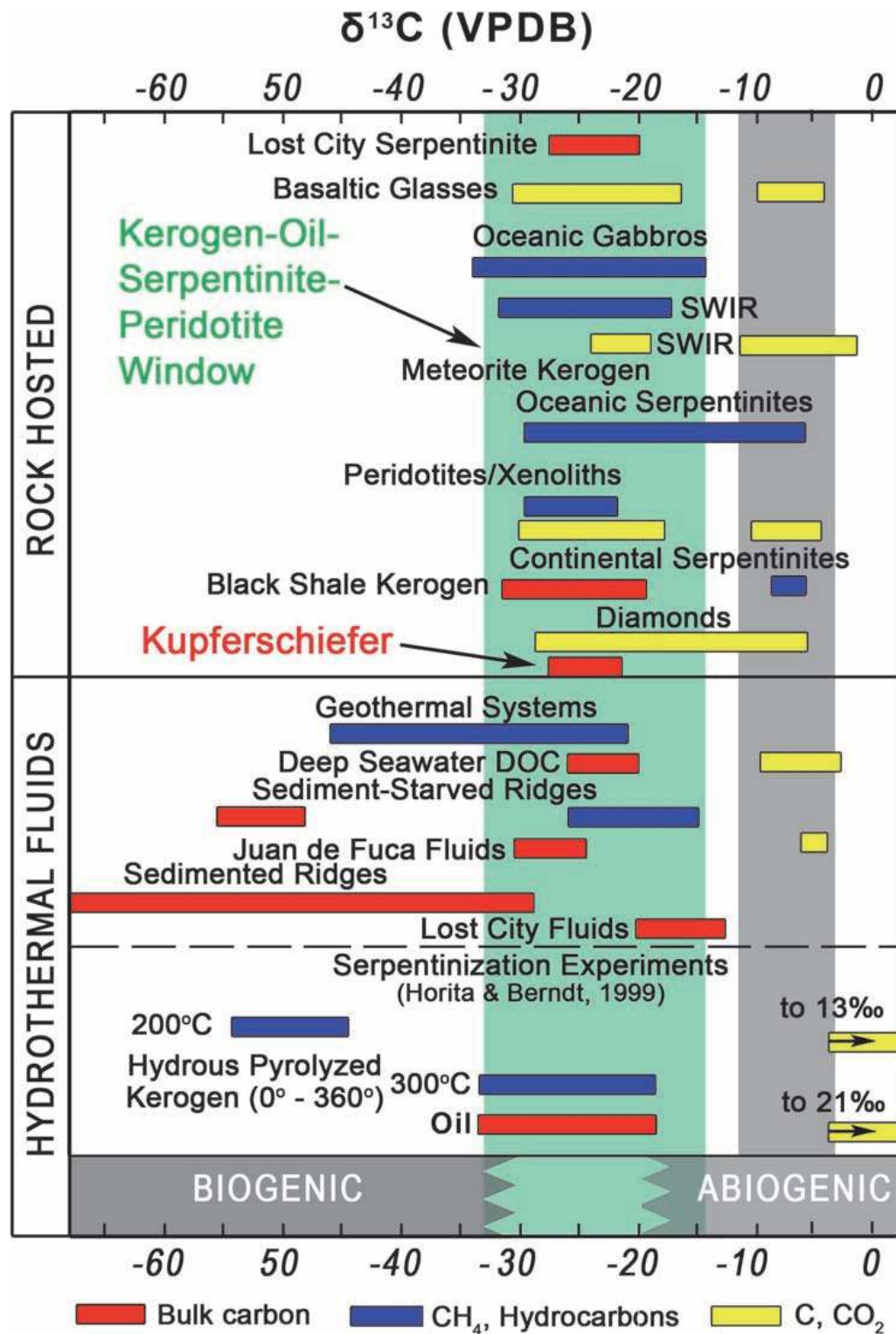


**Figure 6.** Carbon 13 isotopes in the Kupferschiefer compared with  $\delta^{13}\text{C}$  isotope data from world-wide, serpentine-related and other rocks (Kupferschiefer data from [11–14] for Konrad data, [15] for Lost City and other data, [16] for deep seawater, and [17] for basaltic fluids from Juan de Fuca Ridge (as modified from data in [18])).

anomalous and range from  $-42.01$  to  $-44.9\text{‰}$ . In the early-stage chalcocite-digenite-bornite assemblage in the lower to middle Kupferschiefer, sulfur isotopes range between about  $-31$  and  $-40\text{‰}$ .

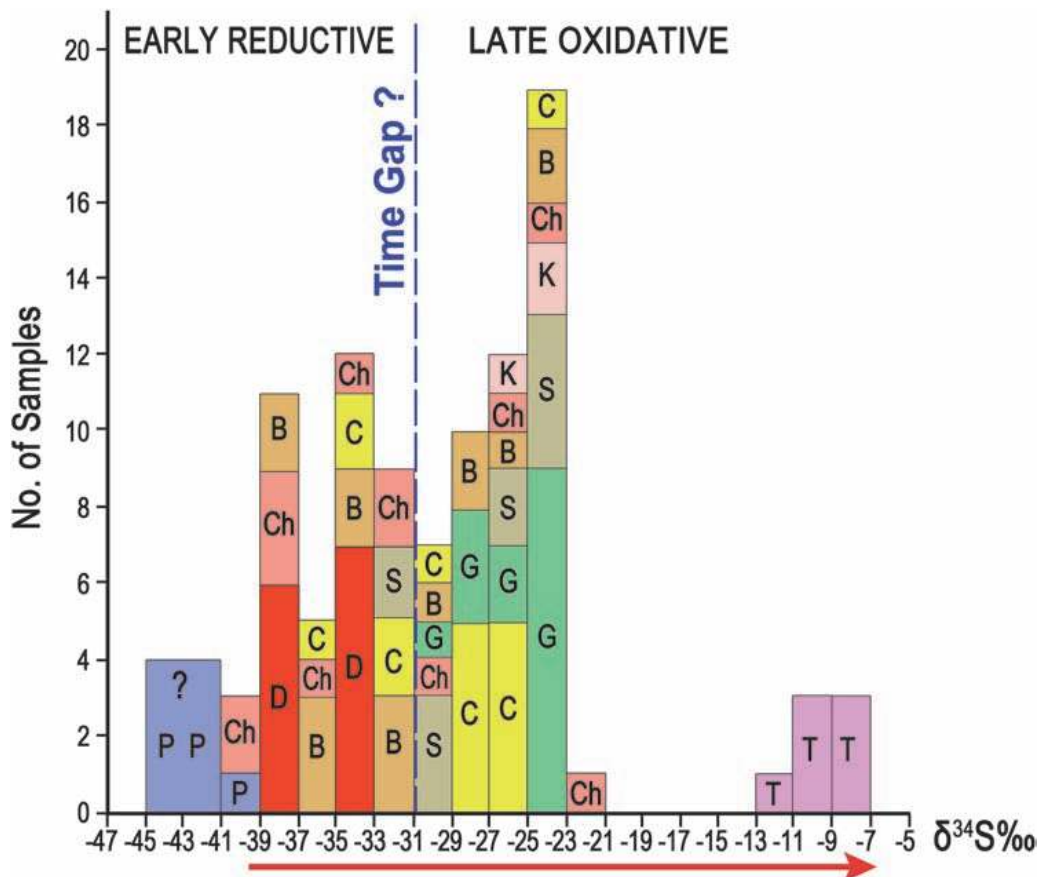


**Figure 7.** Sulfur isotopes at the Lubin copper mine (modified from [19]). Abbreviations: P = pyrite; Ch = chalcocite; D = digenite; B = bornite; C = chalcopyrite; S = sphalerite; G = galena; K = covellite; and T = tennantite-tetrahedrite. Values of  $\delta^{34}\text{S}$  range from  $-10.23$  to  $-7.65$ ‰ for tennantite-tetrahedrite.

In contrast, in the overlying carbonate-marl Kupferschiefer and marl Zechstein carbonates, sulfur isotopes range between  $-31$  and  $-20$ ‰. Presumed late-stage tennantite-tetrahedrite veins exhibit distinct heavy  $\delta^{34}\text{S}$ -enriched sulfur isotopes. Similar sulfur isotope patterns were documented by Spieth [2] in the Kupferschiefer deposit at Spremberg, Germany. Hence, the paragenetic sequence of light reductive sulfur isotopes transitioning upward to heavy oxidized sulfur isotopes for Kupferschiefer types of deposits appears to be a general characteristic of the deposit type.

Given the high temperature of the sulfide mineralization documented by Spieth and Keith and others [1, 2], these low values cannot be explained by microbial reduction. Some other reductive mechanism or source is required. Serpentinization of peridotite is the only other known geologic process that we are aware of that can create light  $\delta^{34}\text{S}$  isotopes (Figure 8). These light  $\delta^{34}\text{S}$  serpentines then become a source for subsequent steatization reactions during mantle heat overprinting, such as may have occurred at the end of the Permian.

Extremely light sulfur isotopes that are associated with late disseminated pyrite in the overlying Zechstein limestones may be explained by low-temperature, conventional microbial reduction in the classic portrayals by Wedepohl [20] for the Kupferschiefer. However at Kupferschiefer, the microbial signature is inferred to be superimposed on an already light sulfur isotope condition that is serpentinite-sourced as in Figure 8.

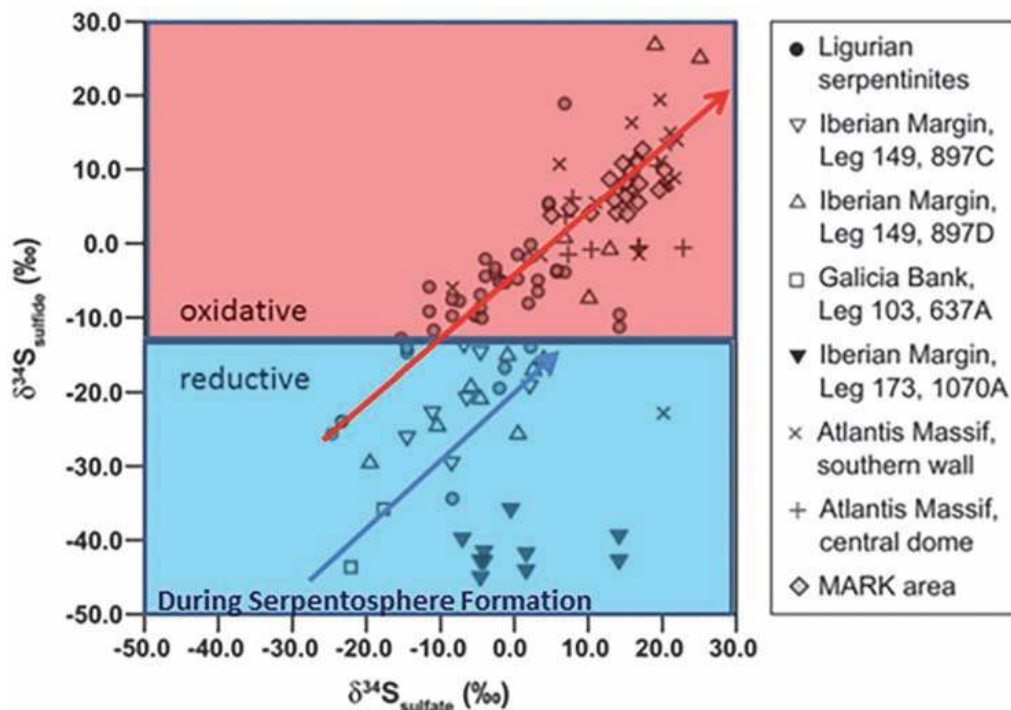


**Figure 8.**  
 Comparison of the sulfide and sulfate isotope compositions of serpentinites from Liguria, the Iberian Margin, the Atlantis Massif, and the MARK area (modified from [19] and including data from references therein).

Only one rock type, oceanic serpentinite, exhibits extremely light sulfur isotopes. When compared with the sulfur isotopes in sulfides in Kupferschiefer rocks [2], it can be argued that brines that were sourced in the serpentine-steatite reaction chamber were buffered at similar low oxidation states. Significantly, oceanic serpentinites have been identified in the Caledonian basement immediately to the southeast of the Lubin and Konrad Kupferschiefer mineral systems southeast of Wrocław.

An upward-lightening sulfur isotope pattern was observed by Sawlowicz and Wedepohl [21] in the Weissliegend sand extrudite mounds at Rudna. The upward-lightening pattern of sulfur isotopes ranged from  $\delta^{34}\text{S}$  of  $-39\text{‰}$  at the bottom of the chalcocite rhythmite section to  $-44\text{‰}$  at the top of a composited rhythmite section. The presence of generally light sulfur isotopes allows the interpretation that deep, serpentinite-sourced brines for the slurries began to deposit chalcocite at the base of the Weissliegend. Hydrogen reduction associated with progressive chalcocite deposition from chloride-hydrogen sulfide brines would have led to production of increasingly lighter  $\delta^{34}\text{S}$  isotopes similar to the broader pattern observed by Kościński in Figure 7 [19] and the light sulfur isotope signature of reduced serpentinite sequences.

#### 2.4 Deep-sourced chemistry and mineralogy in the Zechstein saline succession

Keith and others [1] also hypothesized that much of the saline mass residing in the thick (up to 2000 m), Zechstein saline sequence is not derived from surface evaporative processes, but instead consists of saline, exhalative, chemical, hydrothermal brine products derived from deep serpentinite sources. The concept of a deep serpentine source is supported by the frequent occurrence of talc and magnesium chlorite (clinochlore) in muds, and even serpentine (antigorite) in muds at a number of localities (Figure 1) in the Zechstein [1]. An additional serpentinite mud locality was reported from the Morsleben salt diapir [6]. Both the Morsleben and

Gorleben salt diapirs contain high-lithium brines that were interpreted to represent basement-sourced metamorphic brines [6] and that fit the dehydration narrative discussed below.

Authigenic, Herkimer-habit, quartz crystals contain carnallite in hot, brine fluid inclusions that homogenized at over 200°C in Zechstein salt diapirs. Additional fluid inclusion data reported by Vovnyuk and Czapowski [22] showed that in sylvite-stable, potassium-rich salines, two sets of fluid inclusions were present. The first set ranged from 50° to 62°C, indicating warm hydrothermal conditions attended high-potassium sylvite precipitation from 'basin brines'. The second set ranged from 82° to 135°C, indicating hot hydrothermal conditions. From the perspective of the deep, hot, serpentine-sourced, mud-volcanic model, these brines may have been sourced at much deeper levels in the crust. For example, sylvite has been reported from fluid inclusions in the Weissliegend copper ore, along with potentially primary atacamite reported by Michalik [23].

The rare mineral rokühnite (iron chloride, also known as 'black carnallite') is locally common in carnallite-rich zones at several locations in the Zechstein. To date, rokühnite is not found in other saline localities. The presence of rokühnite may suggest special conditions in the underlying basement whereby both copper and iron were transported in chloride-rich brine to be deposited in overlying carnallite zones of the Zechstein saline sequences.

### 3. Brine source in the serpentosphere

#### 3.1 Description of serpentosphere

Keith and others [24] defined the serpentosphere as a thin (about one to ten kilometers thick), nearly continuous, global-scale layer of serpentinite rock that occurs between the crust and mantle. The serpentosphere is composed mainly (90%) of serpentine group minerals (**Table 2**) [25–27]. An expanded description of the serpentosphere is included here because the serpentosphere concept is important to the Kupferschiefer origin. Chemical compositions of the three main serpentine group minerals were selected by non-chemical criteria by Page [25] and are shown in **Table 2**.

The serpentosphere occurs at the transition between the oceanic crust and the peridotitic mantle, which is widely referred to as the Moho (Mohorovicic geophysical discontinuity). The Moho is characterized by a change in P-wave seismic velocities ( $V_p$ ) that range from 6.8 to 8.2 km/sec (**Figure 9**). These velocities are also characteristic of serpentine, as characterized by petrophysical laboratories. When interpreting seismic velocity profiles and sections,  $V_p$  velocities of 6.8 to 7.3 km/sec indicate lizardite serpentinite and velocities of 7.3 to 7.8 km/sec indicate antigorite serpentinite in serpentinites that have been about 50% serpentinized [26].

Thicker initial serpentosphere material (about 2.5 km thick) may be generated at relatively shallow depths adjacent to slower spreading ridges, such as the Southwest Indian Ridge [28]. Thinner serpentosphere (about 1.5 km thick) may be generated at moderately fast spreading ridges, such as the mid-Atlantic ridge (shown in **Figure 9**).

More recent geophysical work has produced seismic-reflection images of the rocks that comprise the Moho (**Figure 10**). For example, the seismic reflection studies of the northeast Pacific have imaged a reflector layer about 3 km thick beneath a 200 km-long seismic line [29]. The reflectance texture is consistent with shearing that has produced a mylonitic fabric induced by creep of the upper oceanic crust above the peridotitic mantle.

Recent seismic evidence now suggests that the Moho is not simply a geophysical feature, but rather is a thin layer of serpentine-dominated rock. Such rocks have

Major oxide	Chrysotile	Lizardite	Antigorite
SiO <sub>2</sub>	41.53	41.02	42.14
Al <sub>2</sub> O <sub>3</sub>	0.72	1.40	1.64
Fe <sub>2</sub> O <sub>3</sub>	0.72	4.10	1.17
FeO	0.62	0.42	3.73
MgO	40.93	39.44	38.37
H <sub>2</sub> O*	13.54	13.29	12.10
Total	98.03	99.67	99.15
Energy	Low energy		High energy
Temperature	Low temperature		High temperature
Fe <sub>2</sub> O <sub>3</sub> /FeO	1.16	9.8	0.31
Number of samples	31	6	15

**Table 2.**  
 Average composition of serpentine group minerals (data from [25, 27]).

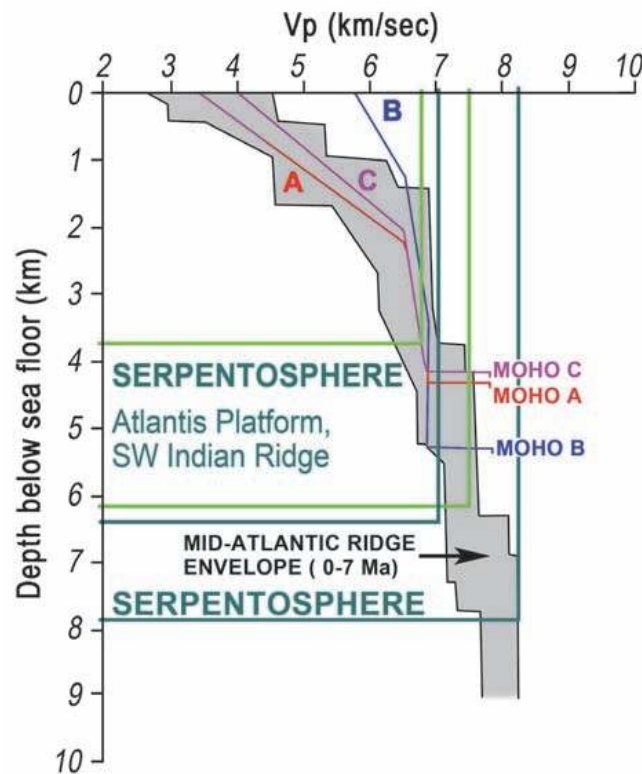


**Figure 9.**  
 Seismic habitats and P seismic wave velocities of the serpentosphere (modified from [28]). Light green lines indicate lizarditic serpentosphere P wave velocities. Dark green lines indicate antigoritic serpentosphere P wave velocities.

been long known, starting with the observations by Steinmann [30] in ophiolite belts that are now sutured into continents. Hess [31] was the first researcher to suggest that there might be a globally distributed layer of serpentinite beneath the ocean basins. Hess noted that serpentine-bearing ophiolites have a world-wide distribution in suture zones within continents [31], which is consistent with the presence of the serpentosphere beneath continental areas.

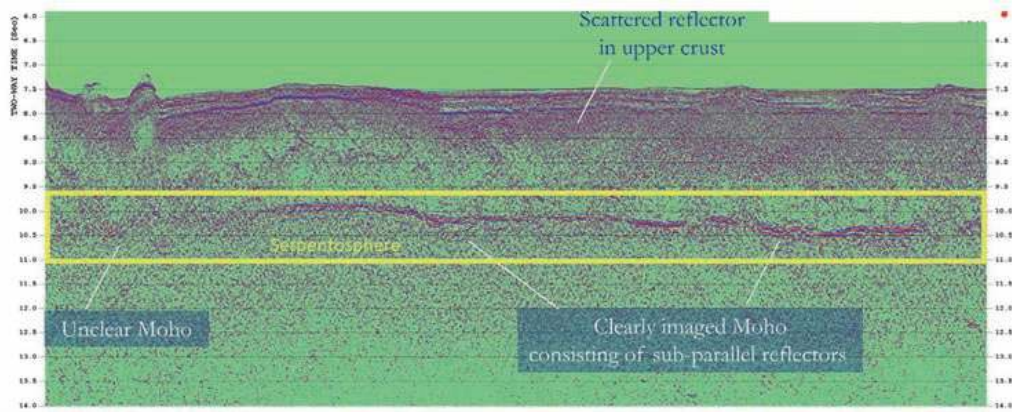


**Figure 10.** Deep seismic image (200 km long) in the northeast Pacific showing the Moho as a zone of subhorizontal reflectors about 3 km thick (modified from [29]).

### 3.2 Tectonic settings of serpentosphere

Serpentosphere occurs in four tectonic settings shown in **Figure 11**. Briefly, serpentosphere is made by hydrolysis of mantle peridotites adjacent to oceanic spreading centers (upper left diagram in **Figure 11**). The serpentosphere is then subducted under normal subduction conditions beneath an asthenosphere-mantle hanging wall (lower left part of diagram), where it sequentially dehydrates to produce hydrous metaluminous arc magmatism in the hanging wall that ultimately intrudes the upper crust to make magmatic arcs.

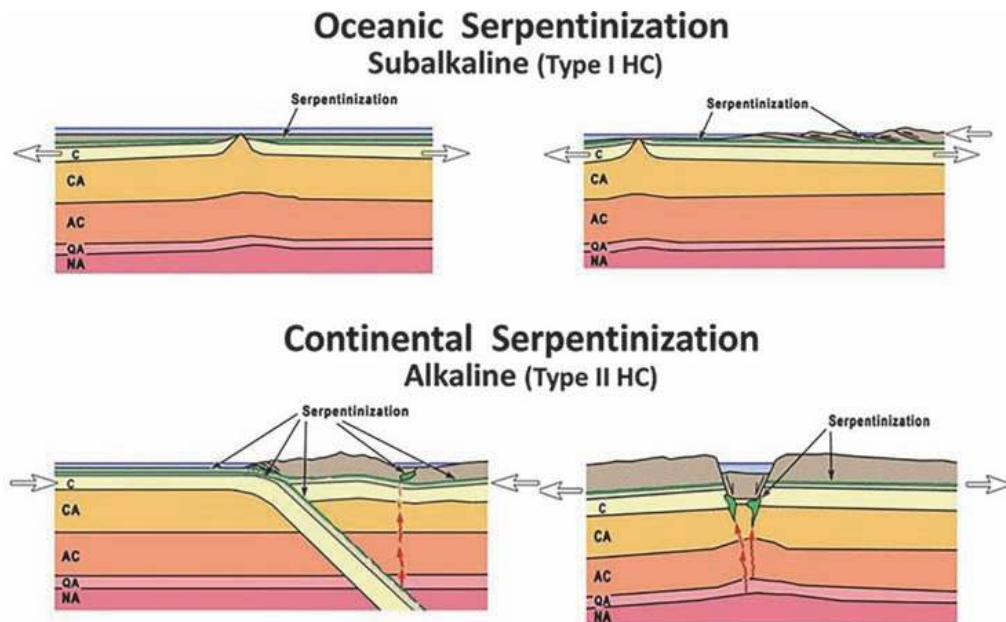


**Figure 11.** Schematic diagrams of four major tectonic settings for the serpentosphere (green line) as discussed in this paper. Upper left: generation of serpentosphere at oceanic rift spreading centers. Lower left: subduction of serpentosphere in normally dipping subduction zones. Upper right: flat subduction of oceanic serpentosphere beneath continental crust during oceanic crust-continent assemblies. Lower right: continental rifting and dehydration of formerly underplated serpentosphere by mantle heating during continental breakups.

A less familiar geotectonic setting is flat subduction beneath typically continental upper plates (upper right part of diagram). In such cases, dehydration of the serpentosphere can produce extensive melting of crustal material in the upper plate to produce peraluminous granitoids.

Subsequent rifting of crust that has experienced previous episodes of flat subduction (lower right part of diagram) can then be systematically dehydrated by mantle heat. The continental rift setting is the tectonic setting envisioned for Kupferschiefer-Zechstein types of deposits.

### 3.2.1 Oceanic rift tectonic settings

Formation of serpentosphere is started near oceanic spreading centers at the mantle-crust contact (**Figure 12** with the explanation in **Figure 13**). Oceanic fluids are pushed down by the weight of the overlying water column into the oceanic fracture system to the contact between the gabbroic oceanic crust layer and the underlying peridotitic mantle. Regional-scale serpentinization reactions occur at that contact and produce low temperature lizardite/chrysotile serpentine [32].

Formation of the serpentosphere results from serpentinization (i.e., hydration) of mantle peridotite by seawater (Eq. (1)). The hydration involves adding water and accompanying elements (especially chlorine and carbon) from the seawater into serpentine. The main serpentine group mineral produced at this stage is the relatively low temperature mineral lizardite, along with magnetite and a brine component. Compared to antigorite, lizardite serpentines are much more oxidized and more hydrous.

Magnetite formation produces considerable hydrogen, which can react with existing carbon in the peridotite to make additional kerogen products, which are shown in Eq. (2). The process is exothermic and heat is released during the reaction. These reactions are important regulators for global climate and, ultimately, hydrothermal hydrocarbon formation.

Simplified serpentinization reaction under supercritical conditions (Eq. (1)).

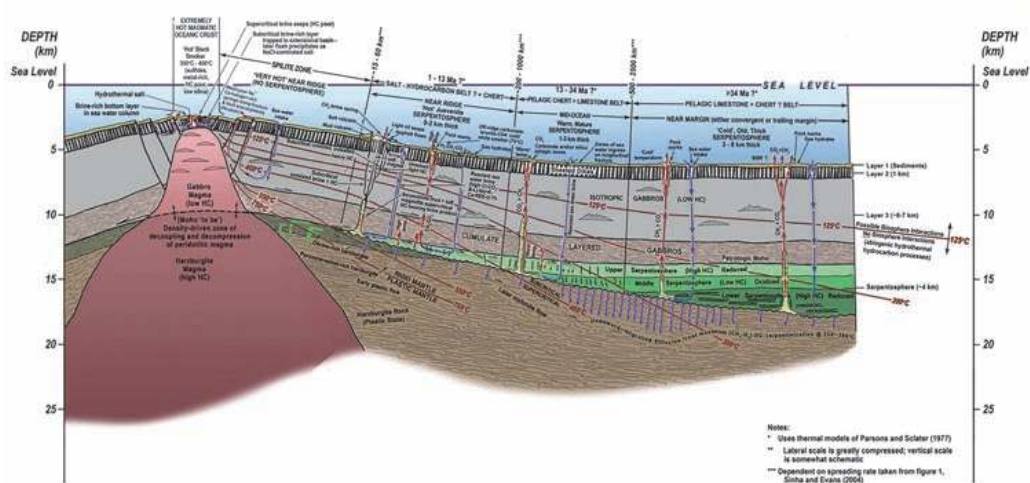
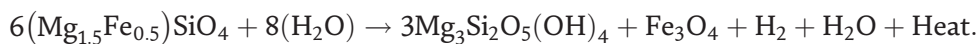


**Figure 12.** Generation of serpentosphere at the oceanic Moho adjacent to oceanic spreading centers (from [33]).

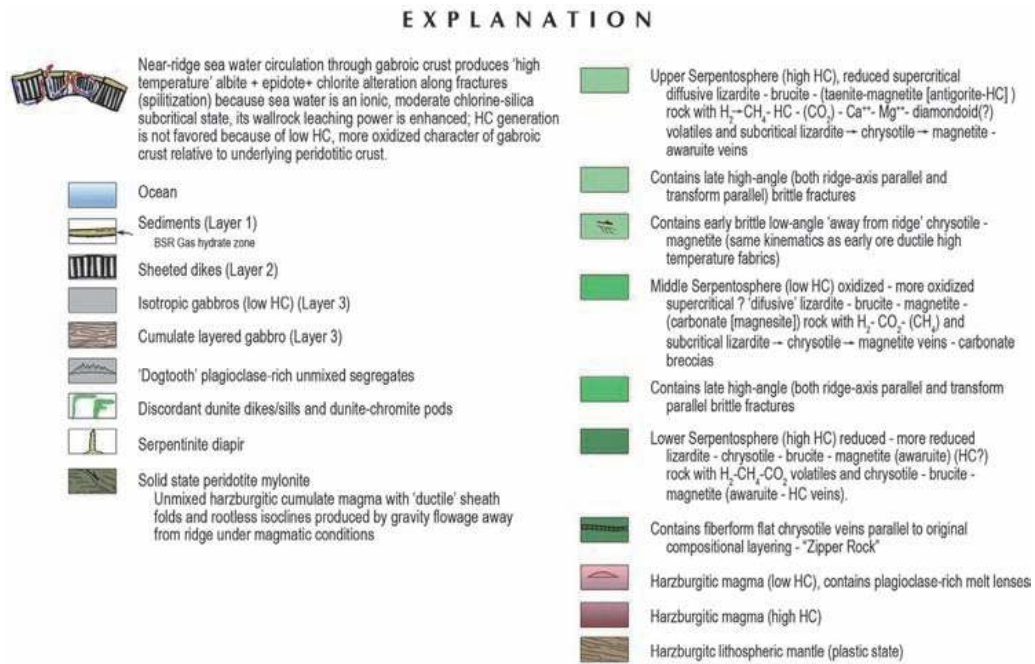
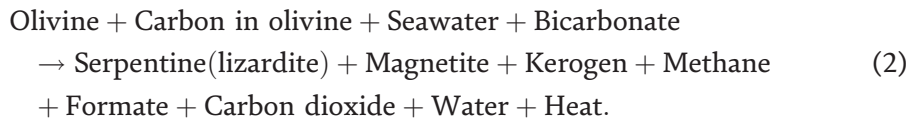
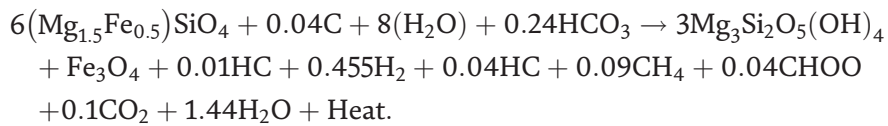


**Figure 13.**  
Explanation for Figure 12.

Simplified serpentinization reaction with carbon under supercritical conditions (Eq. (2)).



Once the serpentinization reaction is initiated, continued seawater flux maintains the reaction. Hence, the thickness of the serpentosphere increases progressively away from spreading centers. At the mid-ocean ridge, serpentosphere thickness is near zero, whereas in oceanic crust adjacent to continents well away from the ridge, serpentosphere thicknesses may range up to 10 km or more.

Lizardite serpentosphere is produced under lower pressure, lower greenschist-grade, hydrothermal, metamorphism/hydration of mantle peridotites in oceanic ridge settings. Brine leakage from this reaction (Eq. (1)) produces white smokers (calcite with minor brucite), such as the white smoker field at Lost City in the central Atlantic Ocean. At the on-ridge setting, oceanic brines leach gabbro to produce sulfide-rich black smokers. The carbon in serpentinite is largely added from seawater as shown in Eq. (2).

The extended serpentine reaction (Eq. (2)) introduces carbon into the serpentine-brine system. The carbon component is probably introduced as bicarbonate or dissolved kerogen (DOC in the literature). These carbon compounds are then reacted into the serpentine-brine product system as varying amounts of dissolved kerogen (HC), methane (CH<sub>4</sub>), formate (CHOO), and carbon dioxide (CO<sub>2</sub>) brine products. Recent literature shows that reduced carbon species are also present in the deep oceans beneath about 2 km [16] and in submarine vents [17].



Both oxidized and reduced carbon sources can be cycled down to the Moho contact where the serpentosphere and its resultant brine products are made. The brine products can then be cycled back up through the overlying oceanic crust to make submarine vents, such as Lost City, and pock marks on the ocean floor.

In this broader perspective, derivative products, such as oil and life, began their evolution in seawater with serpentine as an important mediator. An important link to creation of life is the presence of formate shown in Eq. (2). Formate potentially is the starting platform on which amino acids, RNA, and ultimately DNA can polymerize. The plastic nature of serpentine also functions as a tectonic 'grease' that facilitates plate tectonics.

Compared to the parent peridotite, serpentinites are more magnetic and are lower in density [27]. The coincidence of a magnetic high with a gravity low gives a geophysical signature that can indicate the position of serpentinites at depth beneath or adjacent to ore deposits and oil accumulations, such as richer vents, like Rudna in the Polish Kupferschiefer.

### 3.2.2 Normal-dip subduction tectonic settings

Antigorite serpentosphere is produced via dehydration of lizardite serpentosphere between 300 and 400°C [32] in both normal-dip settings (ocean-continent collisions) and flat subduction settings (continent-continent collisions). The more familiar type of antigorite serpentosphere is formed in normally dipping subduction zones and is later incorporated into alpine collisional orogens as the well-known alpine serpentinites.

### 3.2.3 Flat-subduction tectonic settings

A less familiar type of antigorite serpentosphere is formed in flat or shallowly dipping subduction zones. A detailed schematic of flatly subducting oceanic serpentosphere beneath continental crust is shown in **Figure 14** with the legend in **Figure 15**. Flat subduction of serpentosphere is frequently coupled with trench-directed thrust faults that can provide conduits for deep-sourced brines that were generated during dehydration of the underplating serpentosphere.

An example is the latest Laramide, flat subduction beneath western North America in the Paleocene-Eocene. Kerogen in the flatly subducting serpentosphere is typically a high-hydrogen, Type I kerogen that is linked to Type I petroleum accumulations, such as those found in Wyoming, Colorado, and Utah in the Green River, hypersaline shale horizons. In the case of the Kupferschiefer, flat subduction of the Iapetus Ocean serpentosphere beneath northern Europe occurred 135 Ma earlier, making serpentinite available for later dehydration.

Flat subduction of serpentosphere material is a very under-rated geotectonic process. Mature continental areas are characterized by thick Moho, which may be several times thicker than oceanic Moho. The increased thickness may be due to accumulation of several oceanic serpentosphere layers during numerous, previous, flat subduction episodes at the ends of previous orogenies. These thick serpentosphere layers may be variously dehydrated during subsequent rift episodes associated with continental breakups throughout geologic time.

### 3.2.4 Continental rift tectonic settings

Once serpentospheric materials have been emplaced beneath continental areas by flat subduction, subsequent rifting of the continents creates opportunities for systematic dehydration of the serpentosphere by mantle heat fluxes. Such situations

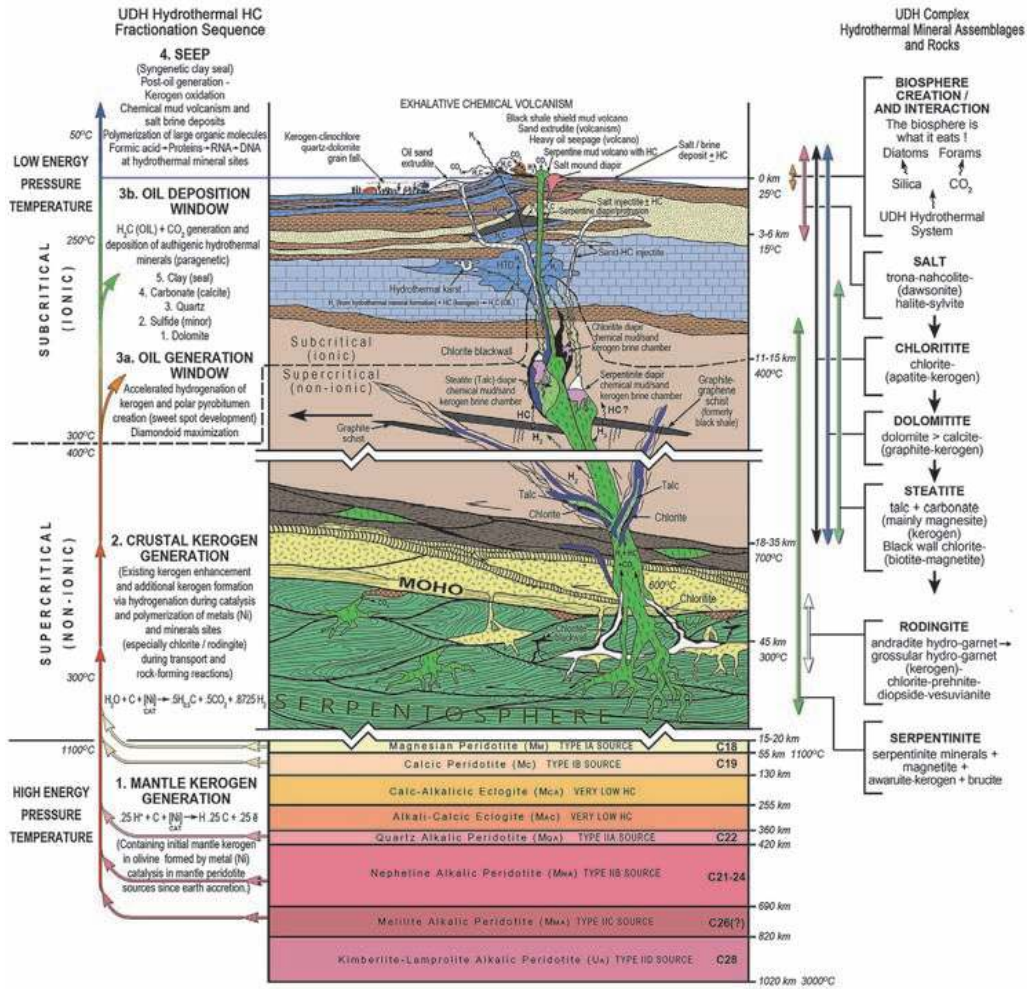


**Figure 14.** Schematic cross section of flat subduction emphasizing southwestern North America features, such as the Green River shales [33]. Explanation is in Figure 15.

occurred in North America and Europe during the breakup of the Pangea supercontinent near the end of the Permian. A schematic cross section of the results of the dehydration and diapiric processes in rift tectonic settings is shown on Figure 16 [1]).

A distinguishing feature of rifting and continental breakups is the penetration of the decompression cone down into the deep, lower mantle asthenosphere. When this deeper penetration occurs, resulting more alkaline diapirs may ascend and interact with the dehydrating serpentospheric material at the base of the rifting and extending continent. These deep interactions may lead to the production of more potassium-rich, alkaline, hydrocarbon deposits (Type II) and their associated brine deposits. These more potassic brines, in turn, lead to the production of much more potassium-rich salines, which precipitate minerals like carnallite and sylvite.

In contrast, in rifting of previously flatly subducted oceanic crust, there is no decompression cone. Instead, shallow, upper mantle, depleted peridotites are hydrated and produce much more sodium-enriched brines that, in turn, lead to sodium-rich trona and nahcolite deposits, such as the Green River hypersaline deposits in the western U.S.

## EXPLANATION



**Figure 15.**  
 Explanation for Figure 14.

### 3.3 Application to kupferschiefer-zechstein sequence

When the above observations are applied to the crust beneath the part of south-western Poland that contains the Kupferschiefer-Zechstein, a deep serpentsphere pattern is present (**Figure 17**). In the central Polish velocity profile shown in **Figure 17**, low-angle, lensoid-shaped packages with  $V_p$  (P-wave) velocities [34]

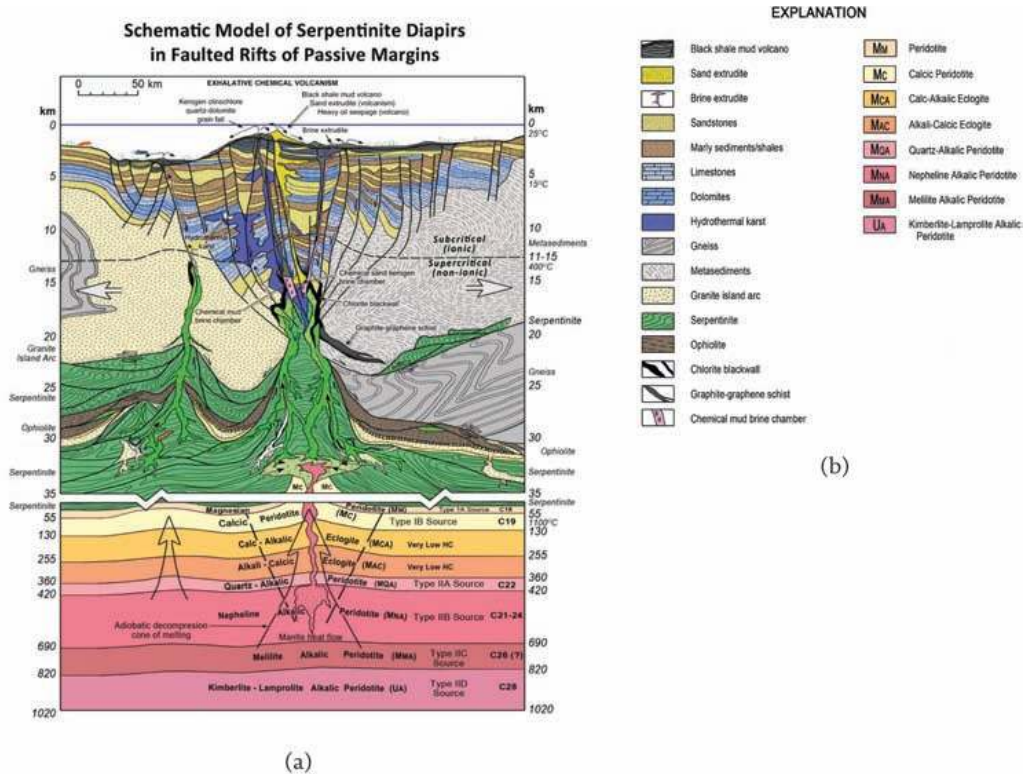


**Figure 16.** Schematic model of serpentine diapirs in rift settings, modeled on the Viking Graben structure in the North Sea between Norway and Great Britain in Kupferschiefer time and explanation (from [1]).

that are consistent with both lizardite and antigorite serpentinites are present beneath southwest Poland.

A more detailed diagram of geophysical profiles for the Lubin area (**Figure 17**) has been modified to show the possible relationship of the Kupferschiefer deposits at Lubin and Konrad to metalliferous plumes originating in continental serpentosphere (expressed by numerous sub-parallel reflectors between 6 and 11 seconds). The plumes utilize a deep-seated fault system, which includes faults that penetrate the crust (such as the Odra fault) and which is indicated by breaks/troughs in the magnetic profile. These are adjacent to the Sudetic block, basement high indicated by the gravity high (**Figure 17**).

Gravity and magnetic profiles for a geophysical line that traverses the Kupferschiefer type deposits on either side of the Fore-Sudetic gravity high [35] show coupled, low-gravity and high-magnetic features are present (**Figure 17**). The gravity low/magnetic high features indicate the possible presence of deep serpentinite. These features may coincide with a deep-seated feeder system that connects deep serpentosphere crust to the Konrad Kupferschiefer system on the south side and the Lubin system on the north side of the Fore-Sudetic high (**Figure 17**).

The importance of deep-seated basement flaws, such as the Odra fault system in Poland, is shown in **Figure 17**. These faults focus heat flow, as well as deep-seated gas fluxes, such as helium that could be generated via serpentinization processes. The presence of such faults can help initiate serpentinite dehydration processes in the lower crust by focusing heat flow from the underlying mantle during continental breakups. An example of continental breakups is the attempted breakup of Pangea in northern Europe in Late Permian. Such a process may have led to development of the Kupferschiefer-Zechstein in the upper crust.

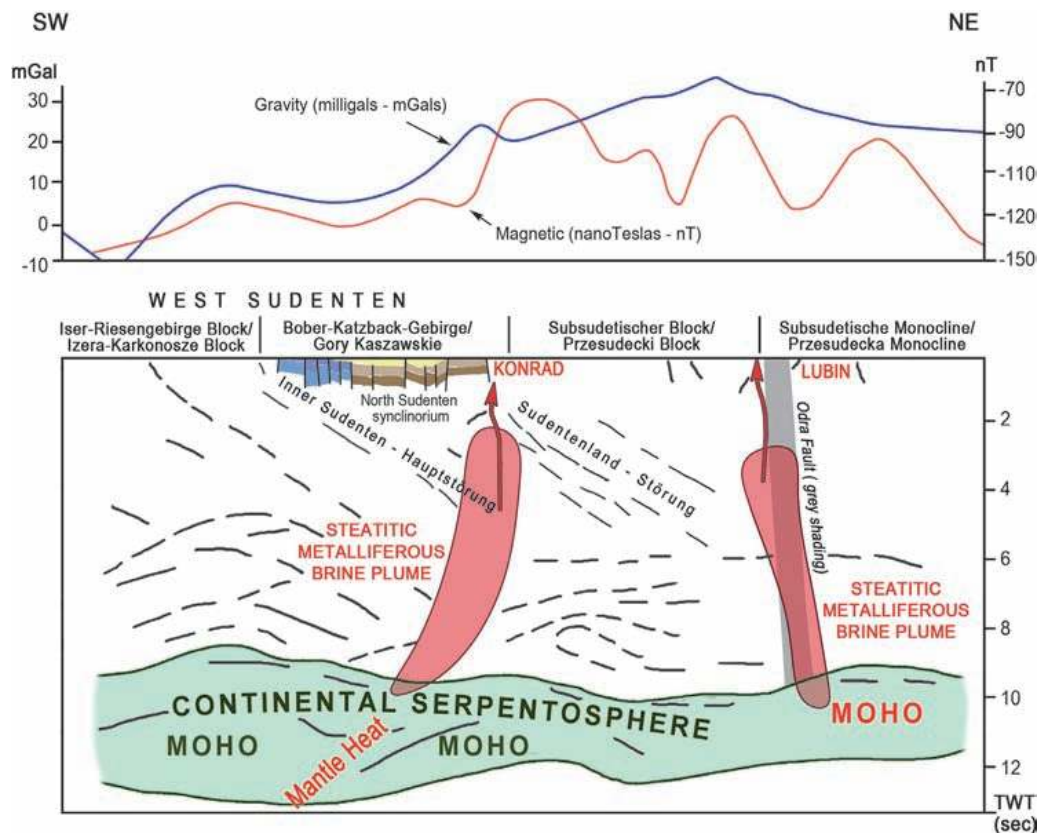


**Figure 17.** Serpentosphere (Moho) beneath Rudna-Konrad-Spremberg Kupferschiefer (modified from [35]).

The position of the Lubin district and the Odra fault projected to the section line is of relevance to the mud-volcanic origin of the Kupferschiefer-Zechstein presented in this article. The Odra fault projection coincides with a prominent deflection of the middle crust velocity packages that extend down to the presumed serpentosphere-velocity lenses in the lower crust (**Figure 18**). For a serpentinite-sourced, ascending, hot brine-mud plume, the upward travel distance is only about 20 km.

Notably, the inferred Caledonide serpentospheric basement is identified in basement massifs southwest of the European Suture zone shown on **Figure 18**, but does not occur to the northeast of the suture. To our knowledge, no Kupferschiefer-type deposits and no deep serpentosphere geophysical signatures are present northeast of this suture. Thus, the European Suture may place an eastern limit on the occurrence of Kupferschiefer-type systems. The lack of Caledonide basement northeast of the European Suture further emphasizes the inference that the presence of serpentosphere is a necessary condition for the occurrence of Kupferschiefer-type systems.

The presence of serpentinite-bearing ultramafic complexes in the basement of uplifts adjacent to Kupferschiefer types of deposits is also important (**Figure 19**). The nearby presence of ultramafic sources, such as the Jordanów-Gogolów serpentinite massif [36], is particularly relevant to the deposits in the Lubin district. Rodingite from this massif was dated at 400 Ma [37]. Fluid inclusions within the dated zircons have yielded homogenization temperatures ranging from 268 to 290° C at about 1 kbar. These data place constraints on the temperatures, pressures, and timing of emplacement of serpentospheric materials in the basement beneath the Kupferschiefer and the hydrothermal event associated with rodingite formation.

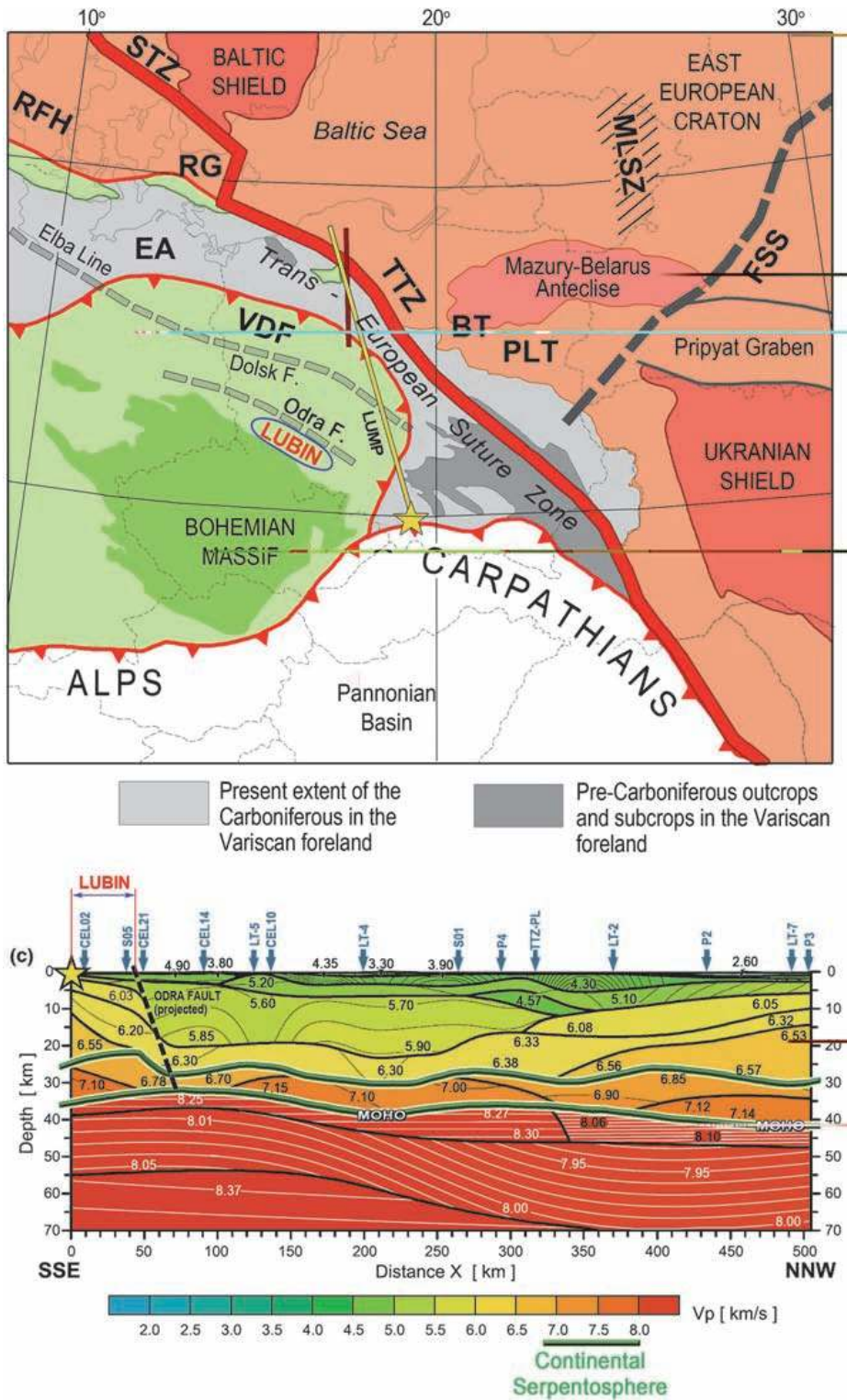


**Figure 18.** Map of Poland and nearby areas showing Teisseyre-Tornquist Zone (TTZ), northeast of which there are no Kupferschiefer type deposits and possibly no underlying Caledonide continental serpentosphere and showing location of the greater Lubin-Kupferschiefer district and its possibly related, deep-seated Odra fault [34]. BT Baltic Terrane, EA Eastern Avalonia, FSS Fennoscandia-Sarmatia Suture, MLSZ Mid-Lithuanian Suture Zone, PLT Polish-Latvian Suture, RG Rønne Graben, RFH Ringkobing-Fyn High, STZ Sorgenfrei-Tornquist Zone, TTZ Teisseyre-Tornquist Zone, VDF Variscan Deformation Front. The area of Bohemian Massif is highlighted in dark green. The Trans-European Suture Zone separates thick and cold Precambrian crust from younger, thin and hot Paleozoic crust. Yellow star shows the location of Libiąż earthquake, which was recorded at LUMP seismic stations. Yellow line shows the LUMP profile (modified from [34]).

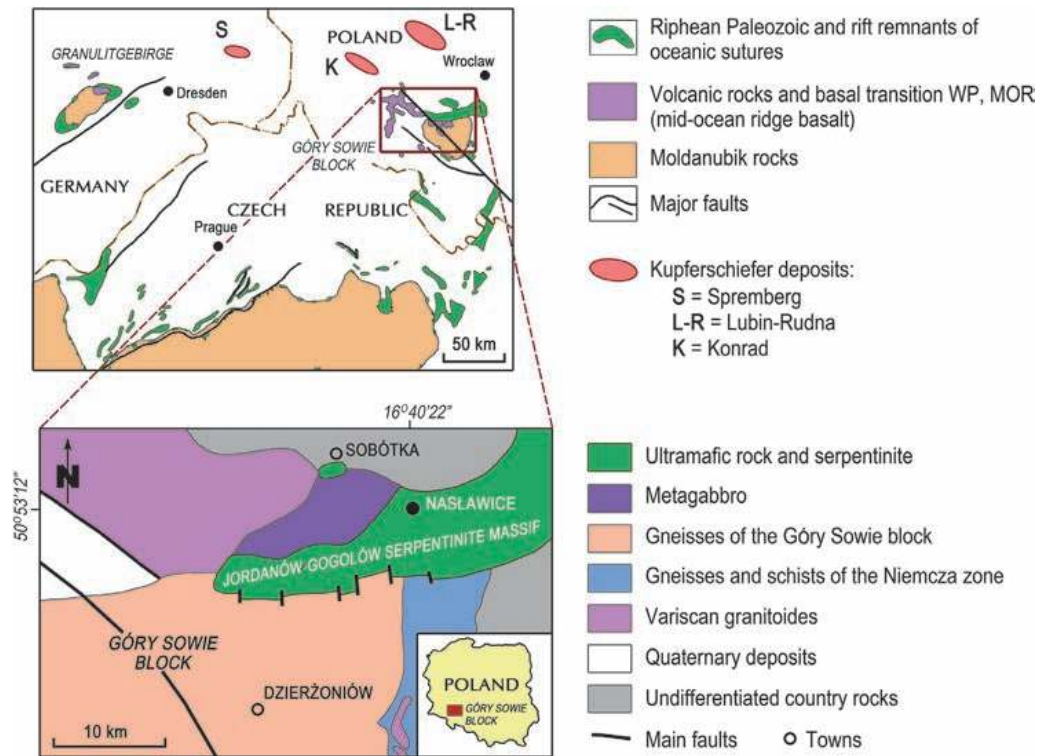


**Figure 19.** Map showing the geographic relationship between the Kupferschiefer deposits and potential ultramafic sources in the Variscan/Caledonide basement (maps modified from [36] and [37]).

The rodingitization event 135 Ma earlier was not the event that created Kupferschiefer mineralization. The serpentosphere emplacement circa 400 Ma, however, was a necessary precursor condition for the ultimate formation of the Kupferschiefer. Without the presence of the Caledonide serpentosphere, the Kupferschiefer could not have happened. During lizarditization of the oceanic peridotites, key ingredients (such as fluorine, sulfur, copper, and others) were added to the lizardite. These elements would later be added to the Kupferschiefer brines during later dehydration events, starting in the uppermost Permian.

With respect to the continental serpentosphere, data suggest that the serpentospheric materials were emplaced beneath northern Europe during the low-angle subduction event of the Iapetus Ocean circa 400 Ma. This material was then affected by mantle-heat-driven dehydration beneath the Odra and related fault systems beginning about 265 Ma, approximately 135 Ma after the emplacement of the Caledonide serpentosphere. The result is hypothesized to be the Kupferschiefer-Zechstein mineralization.

#### 4. Development of a sequential, three-stage dehydration of serpentine in continental rift settings

Results of 15 years of published research in serpentinite terrains, mostly in the Alpine orogen of northern Italy and Switzerland and the Beltic orogen of southern Spain, are summarized in **Figure 20**. This research has identified three episodes of dehydration of serpentinite, as variously presented in [38–42].

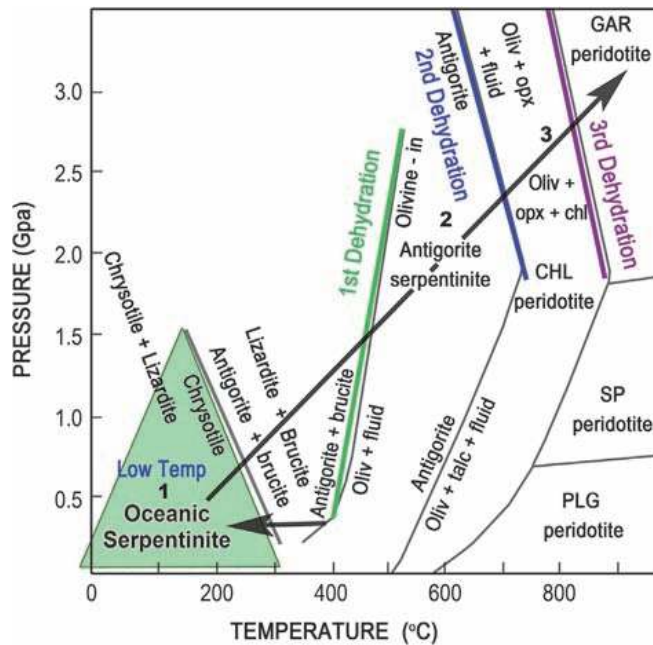


**Figure 20.**

*Pressure-temperature constraints for oceanic lizardite serpentine versus orogenic high-temperature high-pressure antigorite serpentine, higher temperature-pressure chlorite-harzburgite, and highest temperature garnet peridotite showing the first, second, and third dehydration episodes (modified from [38]).*

The three dehydration events are now well documented in serpentinite basements and they can be correlated with the three fluid influxes that built the Kupferschiefer-Zechstein sequence. These papers present a wealth of geochemical data that allowed construction of qualitative mass balance constraints for the chemistry that entered the Kupferschiefer-Zechstein brine during the dehydration episodes and, ultimately, resulted in the brine pulses to the surface.

Four stages of serpentosphere evolution are apparent on **Figure 20** that pertain to evolution of the Kupferschiefer-Zechstein mineralization. The first stage involves hydration of mantle peridotite in oceanic settings within a few km of spreading centers to create low-temperature serpentine. This serpentine ultimately contains the entire anomalous metal suite that characterizes carbonaceous black shales in the Kupferschiefer [39]. The highly anomalous nature of the combined Cu-Ag-Pb-Zn-Mo-Au-PGE-Ni-V-Cr-HC-S kerogeno-metallic system strongly suggests a deep-seated, ultra-deep hydrothermal (UDH), serpentinitized source in the basement. The kerogeno-metallic system correlates with plumes that traveled upward to the seafloor interface via a network of deeply penetrating basement cracks. Various metals are released in a sequential manner through a series of dehydrations.

**Figure 20** also shows the three main dehydration events/processes that correlate with three main depositional events in the Kupferschiefer mineralization:

1. Lizardite to antigorite dehydration creating Weissliegend-Kupferschiefer mineralization (Cu-Ag [Re, Pb, Cl, C, HC]) at 265–255 Ma;
2. Antigorite to chlorite-harzburgite dehydration creating Zechstein saline sequences (Zn-Cu-Pb-Ag [salts: anhydrite, halite, sylvite, etc.]) at 250–234 Ma; and
3. Chlorite-harzburgite to garnet-peridotite dehydration creating Rote Fäule (hematite, muscovite, talc, Au-[PGE-U-Co-Se]) at 245–235 Ma.



The overall metal bias and concentration amounts in the serpentosphere are the same as those elements deposited in the Kupferschiefer black shales (for example, Cu, Ag, Hg, Mo, Co, Ni, V, Sb, U, As). In contrast, elements that are not enriched in the Kupferschiefer and that are close to the average detrital shale composition, typically are not enriched in serpentinites (for example, Ba, Sr, Rb, Sc, Nd, Yb, Lu and Sc, as shown on **Figure 21**).

The apparent correlation of three dehydration events with three metallization events in the Kupferschiefer-Zechstein motivated us to do a more detailed investigation. A major question arising from the above observations is the extent to which element partitioning to the brine phase fits the chemistry of metallization and mineralization patterns in the three stages of Kupferschiefer-Zechstein depositional events.

During this literature study, geochemical information (**Table 3**) was examined that pertained to the initial hydration of mantle peridotite by seawater to serpentine in reaction chambers adjacent to the oceanic ridge system [43–47]. Based on the data, we constructed a series of tables (**Tables 4–7**), from which qualitative mass balance constraints could be determined for sequential brine evolution via dehydration of serpentine in serpentosphere basements.

The elemental data in **Table 4** through **Table 7** are presented as averages. Given the different sources of information, differing numbers of samples, differing analytical procedures, and differing analytical precisions in the various references, the data should be considered qualitative. Nevertheless, there is enough consistency within the classes and enough numerical differences between the classes that we believe that the average results taken from peer-reviewed literature are qualitatively valid.

Many of the anomalous metals from the Kupferschiefer shown in **Figure 21** occur at elevated concentrations in the postulated serpentinite source region in the lower crust. Many of these metals were found during the compilation and were available to be inventoried for their partition into the rock phases or into the brine phases during the various dehydration events. The elements were grouped by their relevance to the sequential brine expulsion model.

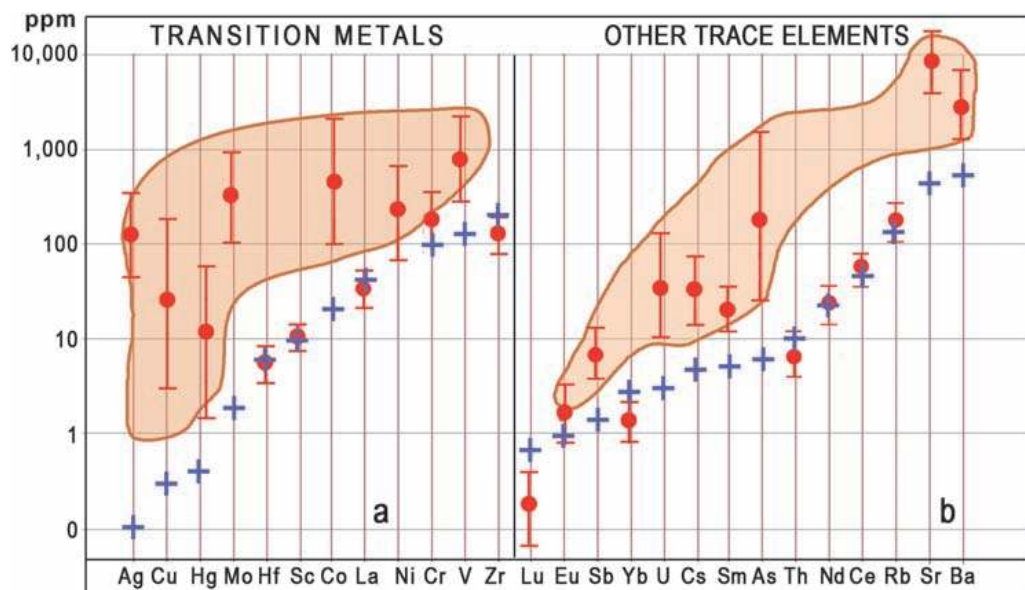


**Figure 21.** Composition of Kupferschiefer shale samples (red dots) showing serpentine-affinity metals and oceanic brine components (pink field) as contrasted with average detrital shale (blue plus signs) (modified from [7]).

Geologic setting/location	Rock type/mineral	Number of samples	Data source
Hydrosphere	Seawater	Average	[45]
Oceanic dunite (fresh) Turkey	Dunite	3	[46]
Oceanic dunite (fresh) Burro Mtn.	Dunite	1	[47]
Oceanic dunite (fresh) Vulcan Peak	Dunite	2	[44]
Oceanic harzburgite (fresh) Turkey	Harzburgite	1	[43]
Oceanic harzburgite (fresh) Burro Mtn.	Harzburgite	3	[47]
Oceanic harzburgite (fresh) Vulcan Peak	Harzburgite	6	[44]
Oceanic serpentinite (lizardite)	Lizardite estimated bulk rock	23	[38]
Low T pre-metamorphic lizardite	Lizardite	7	[40]
Oceanic serpentinite (lizardite)	Lizardite/chrysotile mesh data	46	[41]
Oceanic Serpentinite (lizardite)	Lizardite	4	[42]
High-pressure antigorite serpentinite	Est. bulk-rock amounts	19	[38]
Antigorite high temp. Blueschist	Antigorite	8	[32]
Antigorite (Rhoumejon)4	Antigorite	83	[41]
Antigorite	Antigorite	8	[41]
Olivine-orthopyroxene	Est. bulk-rock amounts	21	[38]
Chlorite-harzburgite	Chlorite-harzburgite	8	[40]
Chlorite-harzburgite	Chlorite-harzburgite	2	[42]
Garnet peridotite	Garnet peridotite	10	[40]

**Table 3.**  
Sources of chemical data used to construct the following tables.

Step	Material	Cl ppm	Li ppm	B ppm	S ppm	C total wt%	Volatile wt %
0	Seawater	19,345	0.17*	4	411	0.003	
0	Average harzburgite-dunite (least altered)	75	1	1	350	0.057	1.7
1	Ave. oceanic lizardite serpentinite	765	3	67	1250	0.82	14.9
	Hydration summary	Huge gain	Big Gain	Huge gain	Huge gain	Huge gain	Huge gain
2	Average antigorite	261	3	39	379	0.08	13.6
3	Average chlorite-harzburgite	45	5	9	812	0.04	1.7
4	Garnet peridotite	n.d.	3	n.d.	n.d.	n.d.	2.7
	Dehydration summary: Gain (goes to rock) and Loss (goes to fluid)	Big loss (3x), then bigger loss (6x)	No pattern	Loss	Big loss, then gain	Big loss, loss	Loss, huge loss, then gain

Note: n.d. = no data.

**Table 4.**  
Brine components - bulk chemical data for serpentinite-related rocks arranged by increasing metamorphic grade (data from [6]).

Step	Material	Cu ppm	Pb ppm	Zn ppm	As ppm	Sb ppm	U ppm
0	Seawater	0.0009	0.00003	0.005	0.0009	Below detection limit	0.0033
0	Average Harzburgite-dunite	16	0.4	44	0.65	0.05	0.05
1	Ave. Oceanic Lizardite serpentinite	22	0.33	43	5	0.17	0.73
Hydration Summary		Slight gain	Slight loss	Same	Gain	Gain	Big Gain
2	Average antigorite	13	0.23	36	3	0.10	0.47
3	Average chlorite-harzburgite	1	0.57	47	0.7	0.05	0.04
4	garnet peridotite	25	2.34	46	18	0.19	0.01
Dehydration Summary: Gain (goes to rock) and Loss (goes to fluid)		Big loss, then gain	Loss, then big gain	Loss, then similar	Loss, big loss, then gain	Big loss, then gain	Big loss

**Table 5.**  
 Base metal components - bulk chemical data for serpentinite-related rocks arranged by increasing metamorphic grade.

Step	Material	MgO wt%	Sc ppm	Ni ppm	Cr ppm	V ppm	Rb ppm	Ba ppm	Sr ppm
0	Seawater	0.217	< 0.000004	below detect. Limit	0.0002	0.0019	8.10	0.02	0.000013
0	Average harzburgite-dunite	46.06	20	1893	2545	28	0.20	1.00	0.47
1	Average oceanic lizardite serpentinite	37.57	6	1830	2154	11	0.20	1.55	8.1
Hydration summary		Loss	Loss	Slight Loss	Loss	Loss	No change	Gain	Huge gain
2	Average antigorite	38.35	6	1015	2168	23	0.25	n.d.	1.95
3	Average chlorite-harzburgite	42.78	11	1753	n.d.	61	0.17	0.39	3.06
4	Garnet peridotite	38.79	19	1513	n.d.	68	0.27	1.77	15
Dehydration Summary: Gain (goes to rock) and Loss (goes to fluid)		No change, then loss	Gain	Gain, then slight loss	No data	Gain	Loss, then Gain	?, then Gain	Large loss, then Gain, then huge gain

**Table 6.**  
 Bulk chemical data for peridotite-related and serpentinite-related rocks arranged by increasing metamorphic grade.

Step	Material	SiO <sub>2</sub> wt%	TiO <sub>2</sub> wt %	Al <sub>2</sub> O <sub>3</sub> wt %	Cr <sub>2</sub> O <sub>3</sub> wt%	MgO wt%	MnO wt %	CaO wt%
0	Average harzburgite - dunite	44.87	0.03	0.66	n.d.	42.67	0.13	1.42
1	Ave. oceanic lizardite serpentinite	41.41	0.06	1.28	0.32	37.57	0.09	0.30
Hydration summary		Loss	Gain	Big gain	?	Loss	Loss	Loss
2	Average antigorite	43.14	0.034	1.01	0.31	38.35	0.089	0.024
3	Average chlorite- harzburgite	42.98	0.034	0.99	0.39	42.69	0.089	0.023
4	Garnet peridotite	43.93	0.13	3.75	0.35	38.79	0.13	3.1
Dehydration summary: gain (goes to rock) and Loss (goes to fluid)		Slight changes	No change then gain	No change then gain	No change	Gain then loss	No change then gain	Huge loss, no change then big gain

**Table 7.**

*Selected whole rock oxide elements, bulk chemical data for serpentinite-related rocks arranged by increasing metamorphic grade.*

Details of locations, rock types, number of samples and sources are presented in **Table 3**. Samples of fresh oceanic peridotite lithosphere were particularly hard to find, which attests to the pervasive nature of serpentinitization at the oceanic crust/Moho contact. Fortunately, field work by Keith located fresh mantle dunites in the Kizildag ophiolite complex in southwest Turkey. Full petrochemical data for these samples are available from the lead author [46].

## 5. Results

Elements partitioned to the brine, which includes Cl, Li, B, S, C, and volatiles (mainly H<sub>2</sub>O), are presented in **Table 4**. Base metals (Cu, Pb, and Zn) and related elements (As, Sb, and U) that are variously enriched in the Kupferschiefer-Zechstein plume events [1] are presented in **Table 5**. **Table 6** presents data for elements that are enriched in peridotite (Mg, Sc, Ni, Cr, V) that might be partitioned to brines that deposit these metals in the Kupferschiefer muds. Also, **Table 6** presents additional information for Rb, Ba and Sr that would be strongly partitioned to the brine component. **Table 7** presents selected whole rock oxide data (SiO<sub>2</sub>, TiO<sub>2</sub>, Al<sub>2</sub>O<sub>3</sub>, Cr<sub>2</sub>O<sub>3</sub>, MgO, MnO, and CaO) that variously reflect elements that may be distributed to the brines that deposited the Kupferschiefer-Zechstein system.

### 5.1 Element gains and losses during formation of serpentosphere

Chlorine and water show the most obvious pattern for evolution from (1) hydration of peridotite to serpentinite, then brine evolution steps (2), (3), and (4) of the sequential dehydration of serpentinite as documented in **Table 4**. The data show that the peridotitic oceanic lithosphere beneath the oceanic crust contains

little water and is hydrated to lizardite serpentinite by the addition of copious amounts of seawater. Chemically, serpentinite is the most hydrated rock on Earth. In oceanic ridge systems, seawater is the only candidate to supply the abundant water, carbon, and chlorine that reside in lizardite serpentine.

The large chemical increases that take place during the conversion of peridotite to serpentinite involve additions of huge amounts of water, halogen, and carbon. Chlorine contents are increased ten-fold, making lizardite serpentinite an excellent candidate for chlorine-enriched brines to supply overlying saline basins. Carbon is augmented twenty-fold, which makes serpentinite an excellent source for hydrocarbon deposits under reduced conditions. In such cases, the carbon travels as reduced, dissolved kerogen (DOC) and is converted to liquid-state hydrocarbons by decompression of the heavy brine fluid in the reservoirs. Water is increased by nine times, making serpentinite the most water-rich major rock type and an excellent source for massive amounts of brine during the dehydration of serpentinite.

In addition, boron and sulfur are added to the rock in abundance and lithium is tripled. Relative to seawater, lithium is at least 15 times higher in serpentinite than in seawater. Hence, serpentinite can provide an abundant source of lithium in brine. Simple evaporation of seawater in the evaporite model does not supply enough lithium as shown in **Figure 22**. The lithium-enriched brines in the Zechstein diapirs clearly contain much more lithium than would be expected to be evaporative products of normal seawater. A metamorphic source for the lithium in Zechstein salines is suggested in [6]. We suggest that serpentinites in the underlying serpentosphere might provide that source.

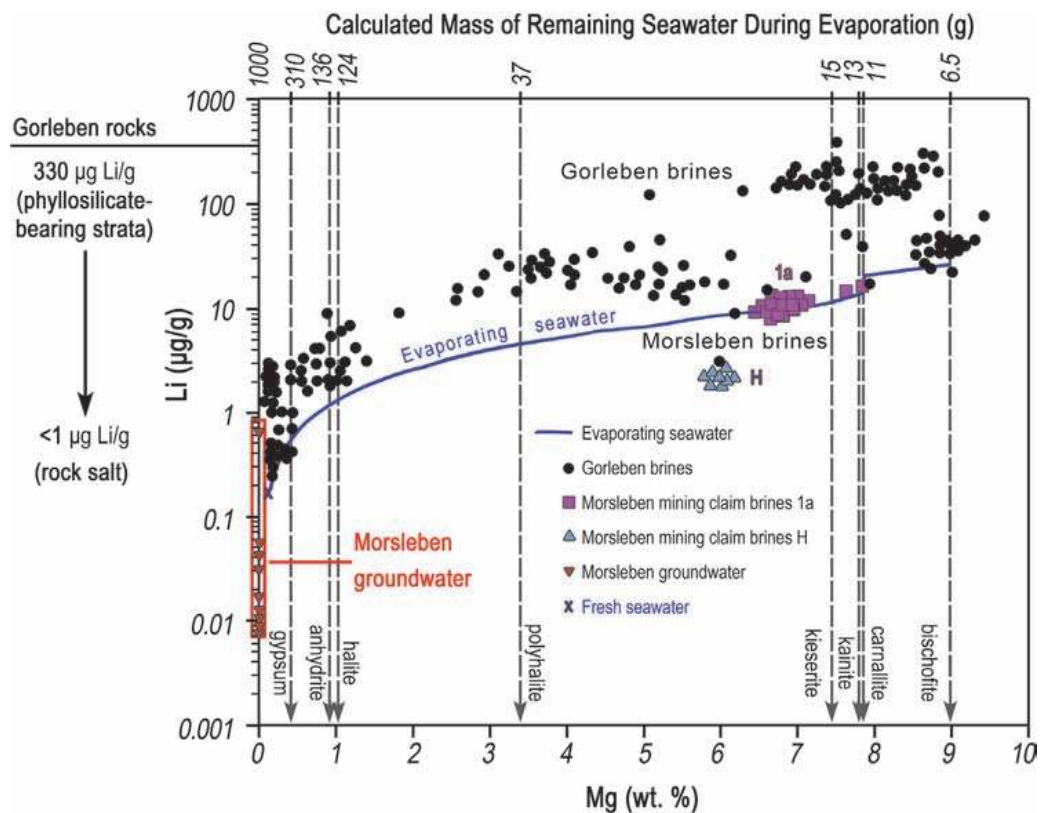


**Figure 22.** Li and Mg concentrations in brine from Gorleben and Morsleben. For comparison, the Li content of the groundwater-monitoring network from Morsleben and the Li content of the rocks from Gorleben are displayed. In addition, the development of the Li content in evaporating seawater (blue line) and the first precipitates from seawater are shown (modified from [6]).

The strong distribution of boron into lizardite serpentinite from boron-poor, fresh peridotite materials indicates that the boron was contributed from the seawater. Hence, the boron in the Zechstein brines is likely to have originated in the seawater that originally made the deep serpentines, and is probably not related to any seawater that might have attended the surface deposition of Zechstein salines.

## 5.2 Gains and losses during dehydration of serpentine

Once the serpentine source is hydrated and loaded with potential brine elements, it undergoes a series of dehydrations whereby the brine elements (Cl, Li, B, S, and C) are distributed to the brine reaction products (**Table 4**). The main volume of saline brines in the Zechstein was produced during the second dehydration event, which is associated with the antigorite to chlorite-harzburgite dehydration. There are five cycles of saline deposition in the second phase of Zechstein chemical sedimentation process.

Similar saline sequences appear in other saline basins, such as the Permian Basin in Texas and Michigan Basin in the USA. Considered on a global scale, based on chlorine data in **Table 4**, it is likely that the second dehydration event of antigorite to chlorite-harzburgite is the most important causal factor in the formation of giant saline deposits.

As the system cooled and collected in mud chambers above the deep source, precipitation of sulfides, such as chalcocite, would have released copious amounts of hydrogen and chlorine, as per the equations in **Figure 2**.

### 5.2.1 Brine element partitioning

Chlorine, on a mass basis, appears to be largely lost from the rock during the dehydration of lizardite to antigorite. However, another approximately 5 times (5x) loss occurs during the dehydration of antigorite to harzburgite. These dramatic differences, originally observed by Scambelluri and others [40], are inferred to relate to fluid loss from serpentine dehydration in normally dipping subduction zones. Flatly subducted serpentosphere has not previously been examined for its contribution to volatile regimes that might be emplaced in the overlying crust above the flatly emplaced serpentinites. Dehydration of these previously flatly subducted serpentinites can also lead to extensive saline releases that are deposited at the Earth's surface in saline basins. The Kupferschiefer-Zechstein sequence is an excellent example of such a process.

In the Kupferschiefer case, the first dehydration provided highly saline brines where any metals that were present would likely have been complexed as metal chlorides. It is also apparent that sulfur is strongly partitioned to the brine component and would have been present in the early Kupferschiefer brines as H<sub>2</sub>S.

Boron appears to be strongly sequestered in the brine component. It is thus not surprising that boron minerals appear in the overlying Zechstein saline sequences, especially in the later cycles. The major loss of boron in the rock occurs in the second dehydration, which helps to explain the occurrence of boron minerals in the later cycles of Zechstein deposition.

Boron and its  $\delta^{11}\text{B}$  isotopes can be used to track the serpentine dehydration reaction in normal subduction zones [48] as shown in **Figures 23–25**. Lizardite begins to break down to antigorite at about 300°C and the reaction is completed by about 400°C at depths of about 40 km under blueschist metamorphic facies conditions. This reaction coincides with a large release of the boron component to the brine (**Figure 23**) and a distinct lightening of the  $\delta^{11}\text{B}$  isotope signature (**Figure 24**)

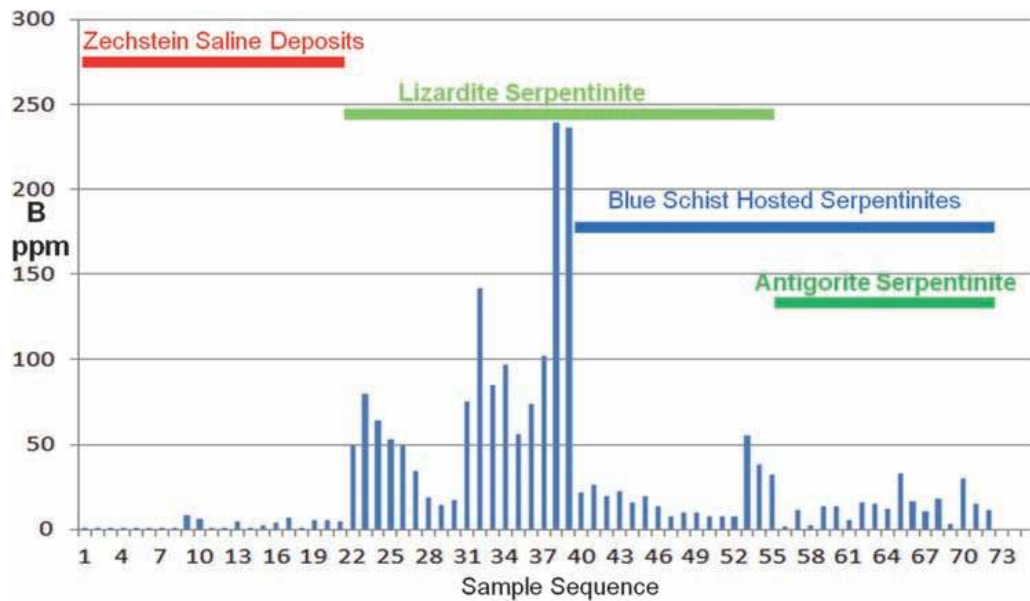


**Figure 23.** Boron concentrations in ppm of Zechstein saline deposits (modified from [49]) and California serpentinites (modified from [48]) and arranged by increasing depth and metamorphic grade.

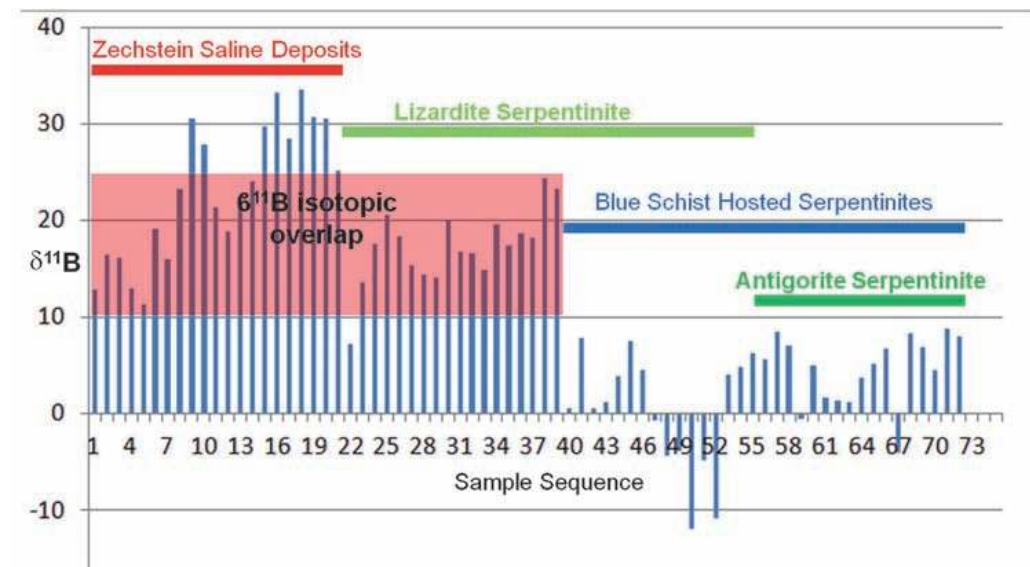


**Figure 24.**  $\delta^{11}\text{B}$  Boron stable isotopes of Zechstein saline deposits (modified from [49]) and California serpentinites (modified from [48]) and arranged by increasing depth and metamorphic grade.

in dehydrated blueschist-associated serpentinite terranes as established for California serpentinites in the Franciscan assemblage [48].

The  $\delta^{11}\text{B}$  isotope signature also strongly overlaps with boron isotopic data reported from brackish to briny water in the Gorleben diapir by [49]. This overlap suggests the saline brines in the Zechstein saline deposits may have been derived from low temperature lizardite sources (below about 300°C) that dehydrated between circa 265 and 240 Ma using the timing presented in [1]. This event would correspond to the 1st and 2nd dehydration events enumerated in this paper. There is a strong overlap between about +24 and +10‰ of  $\delta^{11}\text{B}$  isotopes between unmetamorphosed oceanic lizardite and Zechstein salines. There is also a strong

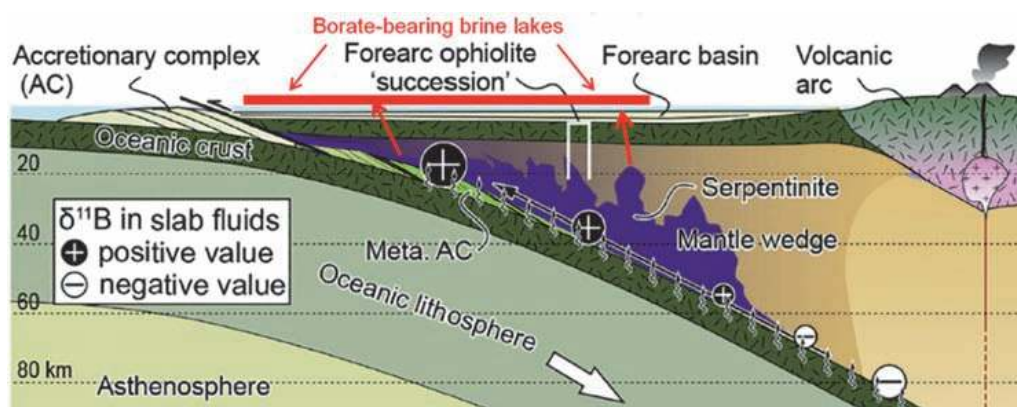


**Figure 25.**

Schematic cross section of a normally developed subduction zone showing a dehydration sequence inferred from boron isotope trends of dehydrating, deep-slab fluids (adapted from [48]). The relative size of '+' and '-' symbols indicates change of the  $\delta^{11}\text{B}$  values; a bold arrow indicates buoyancy-induced flows of serpentinites from deeper portion. Also shown is the inferred position of boron-rich saline lakes, such as those in the California Coast Ranges that may be dehydration products of lizardite that is dehydrating above the descending slab.

lightening of the boron isotope data in blueschist-associated lizardite and antigorite serpentinites.

The hydrogen release is important because hydrogen released from sulfide precipitation is then available to hydrogenate any pre-existing kerogen that might be traveling as a micro-flocculent or dissolved kerogen (DOC) in the brine. Hydrogenation of the probably Polycyclic Aromatic Hydrocarbon (PAH)-enriched kerogen could lead to alkylation and the formation of alkane hydrocarbons and ultimately lead to generation of oil under hydrothermal conditions.

The above observations are consistent with the tenfold decrease in carbon abundance from the lizardite to antigorite dehydration step. This decrease shows that early Kupferschiefer brines would have been very carbonaceous and very hydrogen-rich due to various sulfide precipitation reactions. Not surprisingly, the Kupferschiefer horizon that coincides with the early-stage brine release is the most carbonaceous unit in the Kupferschiefer-Zechstein sequence.

The likely presence of a dissolved kerogen and kerogen flocculent in early Kupferschiefer carbonaceous brine is also supported by the strong partitioning of bulk carbon to the brine component shown in **Table 4**. The presence of the kerogen is also supported by the transfer of bulk carbon from seawater to fresh peridotite during lizardite serpentinite formation (Eqs. (1) and (2)). The presence of reduced carbon, probably as kerogen carbon (the TOC term in chemical analyses) in oceanic serpentinite, also supports the likelihood of a carbonaceous brine source. The presence of carbon is documented by Fröh-Green and others [18] and shown in **Figure 26**. In general, the altered peridotites contain up to five times higher total C-concentrations compared to the oceanic gabbros.

Bulk carbon is non- $\text{CO}_2$  carbon [18] and is likely to be reduced kerogen (HC carbon), because graphite carbon is rare in lizardite serpentinite. The higher reduced carbon content is probably supplied by seawater, where hydrogen is created by formation of magnetite in the serpentinite reaction (Eqs. (1) and (2)). Thus, a significant amount of the bulk carbon released to the brine component, as shown by the data in **Table 4**, is likely to be as kerogen carbon. However, it is also probable that much of this carbon is distributed into carbonate carbon as bicarbonate or dissolved  $\text{CO}_2$ . These carbon compounds are available to precipitate extensive amounts of calcitic and dolomitic carbonate in the overlying, more oxidative, Zechstein saline sequences.



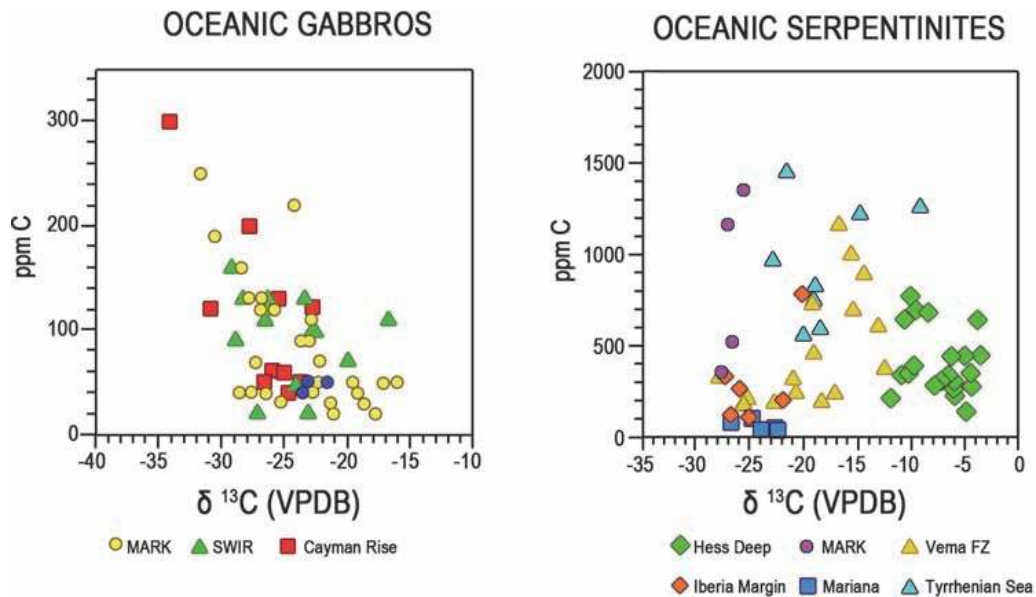


**Figure 26.** Bulk carbon content vs. C-isotope ratios of oceanic gabbros and serpentinites (modified from [18]).

The release of reduced carbon to the brine component during lizardite dehydration to antigorite is consistent with ferric:ferrous ratios of lizardite versus antigorite, as compiled by Page [25] and Coleman [27]. Ferric:ferrous ratios determined for lizardite are 9.8:1 (Table 2). Ferric:ferrous ratios for antigorite are much more reduced with average ferric:ferrous ratio of 0.31:1, which is about 32 times more ferroan. Such reduced ferric:ferrous ratios for antigorite indicate the lizardite to antigorite dehydration occurred under very reduced, hydrocarbon-stable conditions. The brines created under these conditions were very reduced and carried a large component of reduced kerogen capable of reacting to liquid state oil in upper crustal reservoirs. The reduced context of the lizardite to antigorite dehydration helps explain the light sulfur isotopes documented above.

The Kupferschiefer black carbonaceous shales are only one example of a metalliferous, hydrocarbon-rich black shale, and many black shales may have formed this way. These black shales may be chemically distinguished from more aluminum-rich, detrital shales derived from continental granitic sources. Thus, it is an important possibility that carbonaceous black shales in general may have a deep-sourced serpentospheric component.

### 5.2.2 Base metal partitioning

Since 2014, abundant data for copper (for example in Scambelluri and others [40]) now exists throughout all four stages (one hydration stage and three dehydration stages) of the brine generation process (Table 5). Copper is slightly added to oceanic lizardite serpentosphere from average harzburgite-dunite. Harzburgite, which constitutes the main volume of oceanic peridotite, contains an average between 20 and 34 ppm Cu, which indicates that the formation of lizardite serpentine from mainly harzburgitic peridotite was largely isochemical. However, average copper is lost to the brine by about two times from the lizardite precursor during the first dehydration to antigorite. During the antigorite to chlorite-harzburgite dehydration, average copper is lost to the brine by 13x during the second stage of dehydration. Significantly, copper appears to be retained in the garnet-peridotite

rock (perhaps by garnet) during the third dehydration, which would explain the relative absence of copper in the Rote Fäule.

The dehydration sequence for copper explains the copper distribution in the three-fold Kupferschiefer-Zechstein metallized brine sequence. The first two dehydrations produce the copper enrichments observed in the Weissliegend-Kupferschiefer and overlying lower Zechstein (Werra cycle). The third sequence (Rote Fäule) has long been observed to be barren of copper.

Recent literature [1, 2, 50–52] has shown that the Rote Fäule event is a late, overprinting, cross-cutting, copper-poor event. This highly oxidative, hematite-stable, highly acidic event is also copper destructive with respect to the earlier Weissliegend-Kupferschiefer copper mineralization. However, a minor amount of copper might be destroyed and then reprecipitated near the contact with the earlier Kupferschiefer (the so-called 'transition zone').

The copper-poor nature of the late third-stage brine is predicted by the dehydration data. Copper contents change from nearly absent (1 ppm) in the chlorite-harzburgite to much richer (25 ppm) in the garnet peridotite. The combination of strong copper partitioning to the second dehydration event and the distribution of whatever copper might be left to the garnet peridotite leads to the expulsion of a copper-poor brine in the third stage dehydration event. Thus, it is no surprise that the Rote Fäule brine is copper-poor.

Whereas the first two stages of the Kupferschiefer-Zechstein depositions were reduced to highly reduced, the third Rote Fäule stage is highly oxidized and hematite stable. This completely different alteration and metal overprint suggests the appearance of a dramatically more oxidizing brine that overprinted the earlier, more reduced stages. The massive volume of Rote Fäule alteration cannot be explained by a simple change in oxidation state of the pre-existing, more reduced brines that had been previously deposited. The appearance of a third independent, more sulfur-poor, oxidative brine event that was independent of the first two brine events appears to be a simpler alternative than a single hydrothermal event that became oxidized in its later history. The source of this third event would be the third dehydration event induced by chlorite-harzburgite to garnet-peridotite dehydration. Unfortunately, no ferric/ferrous data is yet available for the later dehydration event.

Lead, zinc, arsenic, and antimony display similar patterns to that of copper. They are present in more or less equal levels in the early harzburgite precursor and its hydrated lizardite serpentine product, but are strongly lost to the fluid in the first two stages of brine generation. Whatever is left, however, seems to be captured by the garnet peridotite during the third dehydration, which explains the relative lack of enrichment of these elements in the late-stage Rote Fäule.

Another strong characteristic of the Rote Fäule third dehydration overprint is its overall lack of sulfur (**Table 4**). Sulfur depletion, combined with high oxidation state, explains hematite stability in this sulfur-depleted event. The lack of sulfur in the Rote Fäule coincides with the strong partitioning of sulfur into the garnet-peridotite rock during the third dehydration. The withdrawal of sulfur from participating in third stage brine deposition can largely explain the sulfur depletion that characterizes the oxidized, Rote Fäule hydrothermal plumes.

Whereas the Rote Fäule is barren with respect to familiar Kupferschiefer chemicals such as Cu-S-Pb-Zn-Ag, the Rote Fäule is not barren with respect to other elements. As Pieczonka and Piestrzyński [53] have shown, significant gold resources have been discovered in and immediately adjacent to Rote Fäule (**Figure 27**). The gold mineralization is accompanied by significant platinum group elements (PGE) and uranium. Historically, Rote Fäule was considered the 'death' of copper mineralization and was avoided wherever it was encountered. However, the

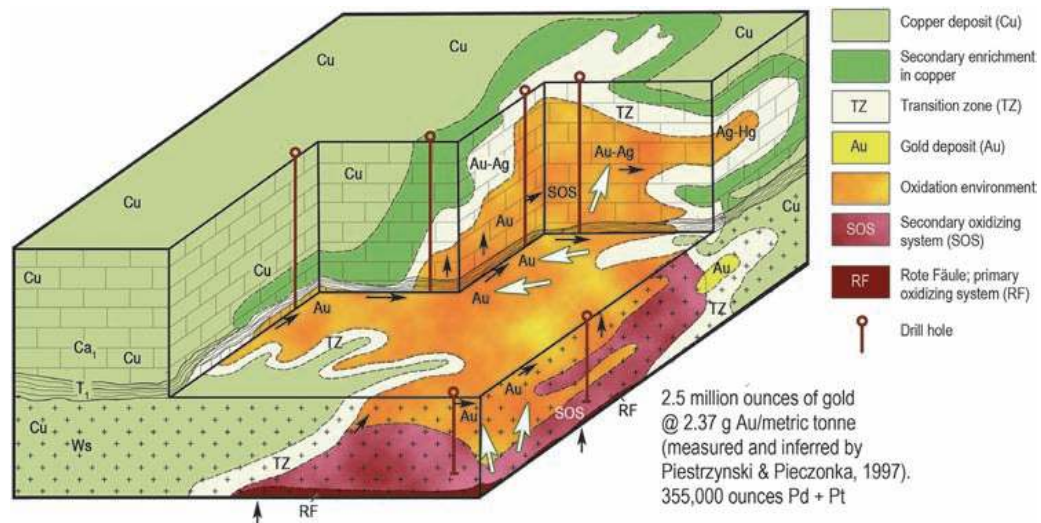


**Figure 27.** Late, noble metal overprint in the Rote Fäule in the Sieroszowice-Polkowice copper mining district, southwestern Poland (modified from [50–52]).

discovery of gold, PGE, and U in the Polish Kupferschiefer points to the potential of Rote Fäule as an economic target in existing Kupferschiefer deposits where mining infrastructure exists or can be rehabilitated (e.g., the Mansfeld-Sangerhausen area in Germany). Unfortunately, no data was uncovered for PGE or Au-Ag during this literature survey.

The uranium enrichment of the Rote Fäule, as well as other parts of the Kupferschiefer, can be explained as resulting from the strong distribution of uranium to the fluids throughout all three dehydrations. Also, uranium was strongly enriched during the initial serpentinization of the harzburgite step. This uranium enrichment implies that seawater was the primary source of uranium in the serpentosphere as peridotites have little or no uranium enrichment. Seawater was likely also the source of uranium for the uranium expelled during the various dehydrations that were deposited in the overlying Kupferschiefer deposits.

### 5.2.3 Peridotite-related element partitioning

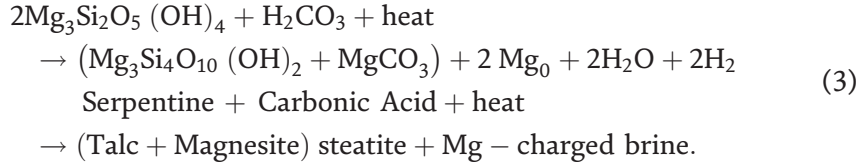
As shown in **Figure 21** and **Table 6**, Kupferschiefer deposits are notable for containing elements common in peridotites, such as Mg, Ni, Cr, and others, which are especially enriched in Kupferschiefer black shale facies. Typical peridotite elements that are enriched and the amount they are increased in Kupferschiefer black shales relative to detrital shale include cobalt (100x), chromium (2x), vanadium (10x), and nickel (5x).

Examination of dehydration data in **Table 6** shows that nickel is lost during the lizardite to antigorite dehydration. Whereas there is little change in chrome in terms of brine enrichment, the brines nevertheless may replicate the relative abundance of elements in the peridotite precursor to the Kupferschiefer-Zechstein mineral deposits. A similar pattern is present for magnesium, whereby magnesium remains relatively unchanged through the dehydration process.

Magnesium enrichments observed in the Kupferschiefer-Zechstein sequence may be related to the process of steatization, where talc is created during dehydration of both lizardite to antigorite and antigorite to chlorite-harzburgite. Steatization can be described by the chemical reaction of Eq. (3). Steatization

releases water and extra magnesium to a brine component and potentially PGE elements, possibly due to volume changes during steatization from larger volumes of serpentine and destruction of PGE-bearing minerals, such as magnetite and awaruite. It is significant that talc has frequently been observed in the overlying Zechstein carbonates (**Figure 1**) [1].

Steatization: serpentine plus carbonic acid goes to talc plus Mg-brine (Eq. (3)).



Zechstein carbonates also show a chemical trend that leads to the magnesium corner on a MgO-KAlO<sub>2</sub>-Al<sub>2</sub>O<sub>3</sub> ternary diagram (**Figure 28**). Much of the data for the chemical muds is derived from magnesium-chloritic muds that are interfingered with salts in the Zechstein sequence as inventoried by Bodine [54].

From the perspective of the deep-sourced, hydrothermal, mud volcanic-brine model, chemical muds derived from deep ultramafic sources contain magnesium-rich minerals like serpentine, clinocllore, talc and tri-octahedral clays (saponite) that were formed in high-density chemical brines. Detrital mud contains continentally derived, aluminum-rich minerals, such as kaolinite, pyrophyllite, and di-octahedral smectite (montmorillonite-beidellite series) clays deposited by sedimentary processes, possibly derived from granitic, continental sources.

Data are also presented in **Table 6** for rubidium, barium, and strontium. These elements are also typical of Zechstein brines [55], as is rubidium enrichment following potassium in muscovite in the lower Kupferschiefer (T-1) unit. In particular, barium and strontium show strong enrichments in the lizardite product of mantle peridotite hydration by seawater. Seawater is probably the source of the barium and strontium. Strontium is then strongly partitioned to the brine component during the lizardite to antigorite dehydration in step 2. Strontium is then also strongly partitioned into the garnet peridotite rock component in step 4. This pattern explains strontium enrichment as strontianite-celestine in the

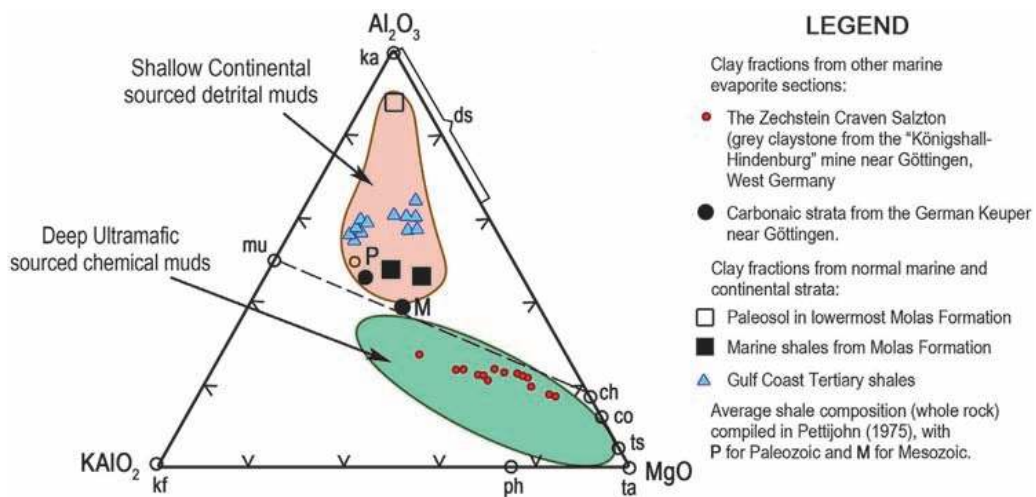


**Figure 28.** Ternary diagram (MgO-KAlO<sub>2</sub>-Al<sub>2</sub>O<sub>3</sub>) showing the contrast between chemical mud from the deep ultramafic mud vs. shallow detrital mud. Green ellipse includes black shale muds from various black shale basins in the continental United States (modified from [54]).

Zechstein saline sequence, where it occurs as celestine that is closely associated with anhydrite mainly in the upper anhydrite unit and in local, crosscutting veins that one-third of the time are associated with talc. Hryniv and Peryt [55] interpreted the veining as derived from brine introduction from a source outside of the saline section. The talc-celestine association is consistent with a possible ultra-deep brine source.

These above enrichments are observed in so-called 'carbonate reef' environments in the middle Zechstein that are associated with hydrocarbon deposition, mainly as gas. The deep-sourced serpentinite model would suggest that both the strontium and hydrocarbons may have a deep source. The enrichment observations also correlate with the mantle helium anomaly documented by Karnkowski [56].

#### 5.2.4 Whole rock oxide partitioning

**Table 7** shows several percent of silica loss and about 25% aluminum loss to the fluid component during the first dehydration from lizardite to antigorite. This observation may help explain the early abundance of silica in the Weissliegend silica extrudite sand unit, as recently reinterpreted by Keith and others [1] and Spieth [2].

The analogous pattern for aluminum helps to explain the presence of early clays in the Weissliegend and especially the muscovitic clays (illite) in the lower Kupferschiefer black shales.

As with sulfides, precipitation of illite clay produces hydrogen. The electrostatic effects at clay layer boundaries also help in the catalyzation of alkane hydrocarbons from more hydrogen-poor, Polycyclic Aromatic Hydrocarbon (PAH)-kerogens that initially enter the system in its early stages. Little change happens during the lizardite to antigorite dehydration (dehydration 1). Aluminum is partitioned into the garnet during the chlorite-harzburgite to garnet peridotite dehydration (dehydration 3). This progressive sequestering of the aluminum component aids in explaining the transition from aluminum-rich materials in the lower part of the Kupferschiefer sequence to the more carbonate-rich materials in the overlying Zechstein cycles.

Calcium shows a dramatic loss to the fluid during the lizardite to antigorite dehydration, which implies that the brines are strongly charged with a calcium component. However as with aluminum, calcium shows little change during the antigorite to chlorite-harzburgite dehydration and is probably partitioned to the garnet peridotite rock during the third dehydration (dehydration 3).

The data suggest that calcium is progressively available throughout the late Kupferschiefer and early stages of Zechstein deposition, and, along with the sulfur change discussed above, calcium is available to make abundant anhydrite in the lower part of the Zechstein in the Werra cycle. As sulfur is continuously partitioned to the brine component during the first and second dehydration, sulfur abundance appears diminished in the upper Zechstein cycles and late Rote Fäule.

## 6. Summary of three dehydration events

Details of the corresponding serpentosphere dehydrations and mineralization stages in the Kupferschiefer are summarized in **Table 8**. The three sequential dehydration events are inferred to have been driven by the input of progressively higher amounts of mantle heat that were focused on deep serpentosphere crust near the base of deep-seated fault conduits, such as the Odra fault system. Based on

Kupferschiefer system formations	Stage	Process	Product of fluid release: metals/ chemistry	Main minerals	Carbon
	Start	Unaltered mantle peridotite generated at spreading centers	Elevated Ni, V, Mg, Cr, Co, PGE, bicarbonate, CO <sub>2</sub> , minor S, K, Ca, Br	Harzburgite rock enstatite and spinel; dunite of olivine, minor spinel	Kerogen in very small amounts
		Seawater	Elevated Cl, Na	Dissolved NaCl	Elevated bicarbonate CO <sub>2</sub>
	Hydration	Add oceanic peridotite + seawater to make lizardite	Add Cl, S, Sr., Ca, Al, C, H <sub>2</sub> O, B, U, Ba, Na	Lizardite serpentine = lizardite + magnetite + minor brucite	Minor calcite, expansion of kerogen component, minor magnesite
Weissliegend-Kupferschiefer	Dehydration 1 releases brine fluids to make Weiss-liegend-Kupferschiefer	Dehydrate lizardite to antigorite	Cu, Ag, early K-Rb, Al, Si, late Ca-Mg, Pb, As, sulfide S, light S isotopes, neutral to mildly acid	bornite, chalcocite-digenite, minor chalcopyrite silica sand, early illite clay, late dolomite marls, late minor calcite	reduced C, kerogen, PAH-enriched
Zechstein	Dehydration 2 releases brine fluids to make Zechstein salines	Dehydrate antigorite to chlorite-harzburgite	Cu-Ag-Pb-Zn, minor As, Sb, Bi; CO <sub>2</sub> , Ca-Mg, high NaCl, max. Sulfate S, sulfide S, heavier S isotopes, mildly acid	major chalcopyrite sphalerite, galena, tennantite, dolomite, anhydrite, later halite, bitumen (oil)	reduced C, alkane-enriched oil, bitumen (oil)
Rote Fäule	Dehydration 3 releases fluids to make Rote Fäule	Dehydrate chlorite-harzburgite to garnet peridotite	Fe (U, PGE, Au, Ag [Cu, Pb, Zn]), very oxidized, very low pH (acid)	hematite, kaolinite, muscovite,	asphaltenic kerogen and PAH

**Table 8.** Stages in formation of Weissliegend-Kupferschiefer to Rote Fäule correlated with corresponding dehydrational stages of the underlying serpentosphere.

extensive studies of dehydrated serpentinites in the Alpine and Beltic orogens, the earlier releases from the serpentines to the brines feature Na, Ca, and Cl, whereas the later releases contain more K, Rb, and Ba. This geochemistry is consistent with the chemo-stratigraphy of the Zechstein, which features more K- and Mg-rich saline brines in the upper cycles.

This study has shown that a mineralogical and geochemical connection can be drawn between the chemical stratigraphy of the Kupferschiefer-Zechstein and the chemistry and mineralogy of the underlying serpentosphere basement that occurs in structurally uplifted blocks between Zechstein ‘basinal’ lows.

The basins are likely created by withdrawal of mud and brine from the underlying mud-volcanic chambers. The connection is further reinforced by a tri-part, pulsed chemical stratigraphy that includes:

1. Chemical mud-brine volcanism (early carbonaceous digenite-chalcocite in Kupferschiefer black shale),
2. Later dolomitic bornite-chalcopyrite-tetrahedrite in Kupferschiefer-Zechstein (with minor sphalerite and galena), and
3. Epigenetic hydrothermal pulses (late hematitic, gold, PGE, minor U) in the Rote Fäule).

This pulsed chemical sequence, at least in part, can be matched with a tri-partite, pulsed dehydrational sequence that may have affected the underlying serpentosphere during Permo-Triassic time. Each pulse reflects a progressive heating and dehydration of the serpentinite basement that released various chemical components that reflect the increased thermal heating. In this mud-volcanic model, the Kupferschiefer-Zechstein sequence represents brine products formed during the first and second dehydration events in the serpentinite basement. In contrast, the Rote Fäule reflects oxidized Fe-Au-PGE (U), high salinity brines driven off during later thermalism associated with the third dehydration event described above.

This deep-sourced, chemical mud volcanic-brine model satisfactorily explains most of the major, often strongly contradictory, observations on the Kupferschiefer-Zechstein. Some of these contradictory juxtapositions include different age dates for different minerals in the same rock and the juxtaposition of high temperature and low temperature mineral assemblages in the same rock. These apparently conflicting observations are ultimately explained by a 'deep-to-seep' model originating in the hot, deep serpentosphere and extruding into a cooler, shallow, seep environment on the shallow sea or lake bottom.

This model of deep-sourced mud-brine volcanism not only explains the Kupferschiefer conundrums, but also explains many other geologic puzzles, for example the origin of oil and other Kupferschiefer analogs, such as the Zambian copper belt. The dehydration model also explains the mass balance problem for salines in salt basins. The evaporative model typically requires too much seawater with a chemical composition different from that observed in many saline basins, especially the Kupferschiefer-Zechstein.

## **7. Conclusions**

The main goal of this paper was to investigate the chemical correlation between the three-fold dehydration sequence of serpentine in the lower crust and the three-fold mineralization sequence in the Kupferschiefer-Zechstein in the uppermost crust. Another goal was to examine evidence for a continental serpentosphere layer beneath Poland and Germany. A final goal was to examine additional evidence, such as carbon and sulfur isotopes in the Kupferschiefer descriptions, for additional evidence of a deep source.

Abundant evidence was found in the geologic and geophysical literature that a continental serpentosphere layer exists as a several km thick layer that has P seismic wave velocities ( $V_p$ ) of 6.8–7.8. Serpentinite is also a common rock in the pre-Carboniferous basement of Caledonide age (380–450 Ma) that exists in the basement massifs adjacent to the Kupferschiefer occurrences.

Regional-scale, deep-seated fault systems, such as the Odra fault, provide a plumbing system through which fluids can ascend from any dehydration events that occurred in the lower crust. These dehydration events acted on the 135-million-years earlier, low-angle, tectonic emplacement of Caledonide ultramafic basement beneath northern Europe.

During the late Paleozoic assembly of the Pangea continent, mantle heat flow focused in the basement and started to dehydrate the underlying ultramafic serpentosphere. The dehydrational, high-density, hot, hydrothermal, mud-brine products were then focused into the deep-seated fracture system. The mud-brine products accumulated as numerous, low-relief, mud-volcanic fields and shallow basins developed on the Permian unconformity above the Rotliegend.

The three-fold dehydration sequence of serpentinite and resulting depositional sequence (**Table 8**) occurred in the following stages:

1. Step 1 dehydration of lizardite to antigorite produced highly reduced, Cu-Ag-Fe-Si-kerogen-chloride-charged brines with elevated Ni, V, Mg, Cr, and Co with very light sulfide  $\delta^{34}\text{S}$  isotopes (265–255 Ma). This first stage dehydration correlates with chemical mud-brine volcanism (early carbonaceous digenite-chalcocite) in the Kupferschiefer black shale.
2. Step 2 dehydration of antigorite to chlorite-harzburgite produced reduced, Cu-Ag-Pb-Zn chloride brines with elevated As, Sb, Bi,  $\text{CO}_2$ , Ca, and Mg with heavier sulfide S isotopes (250–245 Ma). This second stage dehydration correlates with later dolomitic bornite-chalcopyrite-tetrahedrite in Kupferschiefer-Zechstein (with minor sphalerite and galena).
3. Step 3 dehydration of chlorite-harzburgite to garnet produced very acid, very oxidized, hematite-stable Fe, Au, Ag, PGE, REE brines (245–235 Ma). This third stage dehydration correlates with epigenetic hydrothermal pulses (late hematitic, gold, PGE, minor U) in the Rote Fäule.

This sequence, which was hypothesized as a product of dehydration of the basement serpentinite, was examined in more detail by compiling chemical information from a three-fold, dehydrational sequence of serpentinite found in Alpine orogens. Chemistry compiled from the literature, as well as from unpublished MagmaChem data, shows that element distribution into the various brine systems correlates with that found in the three-fold Kupferschiefer depositional sequence.

The first two stages in the sequence contain a high percentage of high-density mud that accumulated as mud volcanoes on the Rotliegend unconformity. The third dehydration stage (Rote Fäule) was much more water-dominated and had lower pH. The Rote Fäule was emplaced as a late-stage overprint that destroyed the pre-existing Weissliegend-Kupferschiefer-lower Zechstein mineralization and replaced it with a hematite-stable Au-PGE-U-enriched mineralization that is not yet fully explored.

The specificity of the deep-seated, hot, hydrothermal, mud-volcanic model provides explanatory power that does not exist in previous, more compartmentalized models. The mud-volcanic model presented here embraces not only the narrow data set of the Kupferschiefer, but also places it in a broader perspective that includes the entire Weissliegend-Kupferschiefer to Zechstein to Rote Fäule sequences.

Beyond its implications for the Kupferschiefer-Zechstein, the ultra-deep hydrothermal (UDH), mud-volcanic model has implications for the origins of the so-called 'red bed copper' model. The red-bed copper deposits can also be interpreted as deep-sourced, chemical, exhalative sediments, with an ultra-deep serpentospheric source for hydrocarbons in general and oil in particular.



## **Acknowledgements**

Much of this research would have been impossible without the generous financial support and intellectual stimulation provided by staff initially at StatOil and later at DetNorske (now Aker BP) companies in Norway. In particular, Hans Konrad Johnsen, Håkon Gunnar Rueslåtten, Martin Hovland, Jens Emil Vinstad, Jon Eric Skeie, and Christine Fichler in Norway and Monte Swan in Evergreen, Colorado, were very helpful. Prof. Massonne and Dr. Tillmann Viefhaus of the Mineralogical Institute at the University Stuttgart, Germany, for many years supported groundbreaking, detailed mineralogical, geochemical, isotopic, and geometallic basic research. Dr. Bernhardt and Dr. J.C. Kopp guided the geological-mineralogical understanding of the German Kupferschiefer occurrences. Recent conversations with Ziegniew Sawlowicz have contributed to our knowledge of the Lubin district. An early review by Martin Hovland significantly improved the manuscript and special illustrations by Peg O'Malley greatly improved the manuscript.

## **Author details**

Stanley B. Keith<sup>1</sup>, Jan C. Rasmussen<sup>2\*</sup> and Volker Spieth<sup>3</sup>

1 MagmaChem Research Institute, Sonoita, AZ, USA


2 Jan Rasmussen Consulting, Tucson, AZ, USA

3 VS.GlobalMetal LLC, Tucson, AZ, USA

\*Address all correspondence to: [mcheme@aol.com](mailto:mcheme@aol.com)

## **IntechOpen**

---

© 2022 The Author(s). Licensee IntechOpen. This chapter is distributed under the terms of the Creative Commons Attribution License (<http://creativecommons.org/licenses/by/3.0>), which permits unrestricted use, distribution, and reproduction in any medium, provided the original work is properly cited. 

## References

- [1] Keith S, Spieth V, Rasmussen J. Zechstein-Kupferschiefer Mineralization reconsidered as a product of ultra-deep hydrothermal, mud-brine volcanism. In: Al-Juboury A, editor, Contributions to Mineralization: InTech; 2018. pp. 23-66. DOI: 10.5772/intechopen.72560
- [2] Spieth V. Zechstein Kupferschiefer at Spremberg and related sites: Hot hydrothermal origin of the polymetallic Cu-Ag-Au deposit [dissertation]. Stuttgart. Germany. Universität Stuttgart. 2019;470. DOI: 10.18419/opus-10530
- [3] Keith SB, Rasmussen JC, Spieth V. Toxic contribution of Kupferschiefer metals, hydrocarbon and related Zechstein salines to the Permian extinction event (abstract). SGA, Glasgow Conference, August. 2019; 26-30
- [4] Zientek ML, Oszczepalski S, Parks HL, Bliss JD, Gorg G, Box SE, et al. Assessment of undiscovered copper resources associated with the Permian Kupferschiefer, Southern Permian Basin, Europe. U.S. Geological Survey Scientific Investigations Report. 2015;SCI-2010-5090-U:1-94
- [5] Czapowski G, Bukowski K. Salt resources in Poland at the beginning of the 21st century. *Geology, Geophysics & Environment*. 2012;**38**(2): 189-2008
- [6] Mertineit M, Schramm M. Lithium occurrences in brines from two German salt deposits (Upper Permian) and first results of leaching experiments. *Minerals*. 2019;**7**:66:1-21. DOI: 10.3390/min9120766
- [7] Lewan MD. Experiments on the role of water in petroleum formation. *Geochimica et Cosmochimica Acta*. 1997;**61**(17):3691-3723
- [8] Lewan MD, Kotarba MJ, Wieclaw D, Piestrzynski A. Evaluating transition-metal catalysis in gas generation from the Permian Kupferschiefer by hydrous pyrolysis. *Geochimica et Cosmochimica Acta*. 2008;**72**:4069-4093
- [9] Kucha H. Geology, mineralogy and geochemistry of the Kupferschiefer, Poland. In Irish Association for Economic Geology. Special Volume on Europe's Major Base Metal Deposits. 2003:215-238
- [10] Blundell DJ, Karnkowski PH, Alderton DHM, Oszczepalski S, Kucha H. Copper mineralization of the Polish Kupferschiefer: A proposed basement fault-fracture system of fluid flow. *Economic Geology*. 2003;**98**: 1487-1495
- [11] Sawłowicz Z. Cu-Ag deposits on the Fore-Sudetic monocline, Poland (Kupferschiefer type). Power point. Jagiellonian University, Krakow, Poland. 2017; Contribution No. 1364
- [12] Sawłowicz Z. Organic matter in Zechstein Kupferschiefer from Fore-Sudetic Monocline (Poland). I. Bitumens. *Mineralogia Polonica*. 1989; **20**(2):69-87
- [13] Sawłowicz Z. Primary copper sulphides from the Kupferschiefer, Poland. *Mineralium Deposita*. 1991;**25**: 262-271
- [14] Püttmann W, Hageman HW, Merz C, Speczik S. Influence of organic material on mineralization processes in the Permian Kupferschiefer Formation, Poland. *Advances in Organic Geochemistry Organic Geochemistry*. 1988;**13**(1-3):357-363
- [15] Lang SQ, Butterfield DA, Schulte M, Kelley DS, Lilley MD. Elevated concentrations of formate, acetate and

dissolved organic carbon found at the Lost City hydrothermal field. *Geochimica et Cosmochimica Acta*. 2010;**74**:941-952

[16] Druffel ERM, Williams PM, Bauer JE, Ertel JR. Cycling of dissolved and particulate organic-matter in the open ocean. *Journal of Geophysical Research*. 1992;**97**:15639-15659

[17] Lin H-T, Repeta DJ, Xu L, Rappes MS. Dissolved organic carbon in basalt-hosted deep seafloor fluids of the Juan de Fuca Ridge flank. *Earth and Planetary Science Letters*. 2019;**513**: 156-165

[18] Früh-Green GL, Connolly JAD, Plas A. Serpentinization of oceanic peridotites: implications for geochemical cycles and biological activity. In *The Seafloor Biosphere at Mid-Ocean Ridges*. American Geophysical Union, Geophysical Monograph Series. 2004;**144**:119-136

[19] Kościński M. Diversity of the sulfur isotopic composition in the individual sulfide minerals from the copper Lubin Mine, SW Poland. *Mineralogical Society of Poland Special Papers*. 2003; **23**:96-98

[20] Wedepohl KH. Composition and origin of the Kupferschiefer bed. *Geological Quarterly*. 1994;**38**(4): 622-658

[21] Sawłowicz Z, Wedepohl KH. The origin of rhythmic sulphide bands from the Permian sandstones (Weissliegendes) in the footwall of the Fore-Sudetic “Kupferschiefer” (Poland). *Mineralium Deposita*. 1992;**27**: 242-248

[22] Vovnyuk SV, Czapowski G. Generation of primary sylvite: The fluid inclusion data from the Upper Permian (Zechstein) evaporates, SW Poland. In Schreiber BC, Lugl S, Babel M. editors. *Evaporites through Space and Time*.

Geological Society, London, Special Publications. 285:275-284

[23] Michalik M. Chlorine containing illites, copper chlorides and other chlorine bearing minerals in the Fore-Sudetic copper deposit (Poland). In: Papunen H, editor. *Mineral Deposits*. Rotterdam: Balkema; 1997. pp. 543-546

[24] Keith SB, Swan M, Rueslatten H, Johnsen HK, Page N. The serpentosphere. *Geological Society of Nevada Newsletter*. 2008;**23**(3):3

[25] Page NG. Chemical differences among the serpentine “polymorphs”. *American Mineralogist*. 1968;**53**:201-215

[26] Christiansen NI. Serpentinities, peridotites, and seismology. *International Geology Review*. 2004; **46**(9):795-816

[27] Coleman RG. Petrologic and geophysical nature of serpentinites. *Geological Society of America Bulletin*. 1971;**82**:897-918

[28] Muller MR, Robinson CJ, Minshull TA, White RS, Bickle MJ. Thin crust beneath ocean drilling program borehole 735B at the Southwest Indian Ridge. *Earth and Planetary Science Letters*. 1997;**148**:93-107

[29] Kodaira S. Oceanic Moho and mantle: What we learned from recent active source seismic studies: Reaching the Mantle Frontier: Moho and Beyond. 2010. Washington, D.C. 21

[30] Steinmann G. *Geologische Beobachtungen in den Alpen. II: Die Schardt'sche Überfaltungstheorie und die geologische Bedeutung der Tiefsceabsätze und der ophiolithischen Massengesteine*. Ber. Nat. Ges. Freiburg. 1905;**i**(16):44-65

[31] Hess HH. History of ocean basins. In: Schreiber BC, Harner HL, editors.

Petrologic Studies: A Volume to Honor A.F. Buddington, November. Boulder, Colorado, USA: Geological Society of America; 1962:599-620

[32] Schwartz S, Guillot S, Reynard B, Lafay R, Debret B, Nicollet C, et al. Pressure-temperature estimates of the lizardite/antigorite transition in high pressure serpentinites. *Lithos*. 2013;**178**: 197-210

[33] Keith SB, Swan MM. Generation of normal oceanic serpentosphere. In: Unpublished poster, MagmaChem Exploration. Sonoita, Arizona, USA: MagmaChem Research Institute; 2008. p. 1. Available from: [www.MagmaChemRI.org/](http://www.MagmaChemRI.org/)

[34] Dec M, Polkowski M, Janik T, Stec K, Grad M. Verification of P-wave velocities under Moho boundary: Central Poland case study, LUMP profile. *Acta Geophysica*. 2018;**12**. DOI: 10.1007/s11600-018-0236-9

[35] Kopp J. Personal Communication. Potsdam, Brandenburg, Germany: Kopp Consulting; 2018

[36] Dubińska E, Gunia P. The Sudetic ophiolite current view on its geodynamic model. *Geological Quarterly*. 1997;**41**(1):1-20

[37] Dubińska E, Bylina P, Kozłowski A, Dörr W, Nejbort K, Schastok J, et al. U-Pb dating of serpentinitization: Hydrothermal zircon from a metasomatic rodingite shell (Sudetic Ophiolite), Southwest Poland. *Chemical Geology*. 2004;**203**:183-203

[38] Scambelluri M, Fiebig J, Malaspina N, Muntener O, Pettke T. Serpentine subduction: Implications for fluid processes and trace-element recycling. *International Geology Review*. 2004;**6**:595-613

[39] Spieth V, Trinkler M, Kopp B, Keith SB, Rasmussen JC. Hot, deep-

sourced, hydrothermal Cu-Ag-Au-PGE-polymetallic deposits of the Zechstein-Kupferschiefer age (abstract). Glasgow, Scotland: SGA Conference; 2019

[40] Scambelluri M, Pettke T, Rampone E, Godard M, Reusser E. Petrology and trace element budgets of high-pressure peridotites indicate subduction dehydration of serpentinitized mantle (Cima di Gagnone, central Alps, Switzerland). *Journal of Petrology*. 2014;**55**(3): 459-498

[41] Rhoméjon S, Andreani M, Früh-Green GL. Antigorite crystallization during oceanic retrograde serpentinitization of abyssal peridotites. *Contributions to Mineralogy and Petrology*. 2019; **174**(60):1-25

[42] Alt JC, Schwarzenbach EM, Früh-Green GL, Shanks WC, Bernasconi SM, Garrido CJ, et al. The role of serpentinites in cycling of carbon and sulfur: Seafloor serpentinitization and subduction metamorphism. *Lithos*. 2013;**178**:40-54

[43] Engin T, Hirst DM. Serpentinisation of harzburgites from the Alpine peridotite belt of southwest Turkey. *Chemical Geology*. 1970;**6**:281-295

[44] Himmelberg GR, Loney RA. Petrology of the Vulcan Peak alpine-type peridotite, southwestern Oregon. *Geological Society of America Bulletin*. 1973;**84**:1585-1600

[45] Anthoni JF. The Chemical Composition of Seawater. Leigh R.D.5, New Zealand: Seafriends Marine Conservation and Education Centre, 2006. Available from: [www.seafriends.org.nz./ocean/seawater.htm](http://www.seafriends.org.nz./ocean/seawater.htm)

[46] Keith SB. MagmaChem data files, available on MagmaChem Research Institute website. <http://MagmaChemRI.org>

- [47] Loney RA, Himmelberg GR, Coleman RG. Structure and petrology of the alpine-type peridotite at Burro Mountain, California. U.S.A. *Journal of Petrology*. 1971;**12**(2):245-309
- [48] Yamada C, Tsujimori T, Change Q, Kimura JI. Boron isotope variations of Franciscan serpentinites, northern California. *Lithos*. 2019;**334-335**: 180-189
- [49] Kloppmann W, Negrel P, Casanova J, Klinge H, Schelkes K, Guerrot C. Halite dissolution derived brines in the vicinity of a Permian salt dome (N German Basin): Evidence from boron, strontium, oxygen, and hydrogen isotopes. *Geochimica et Cosmochimica Acta*. 2001;**65**(22): 4087-4101
- [50] Piestrzyński A, Sawłowicz Z. Exploration for Au and PGE in the Polish Zechstein copper deposits (Kupferschiefer). *Journal of Geochemical Exploration*. 1999;**66**:17-25
- [51] Piestrzyński A, Wodzicki A. Origin of the gold deposit in the Polkowice-West Mine, Lubin-Sieroszowice mining district. Poland. *Mineralium Deposita*. 2000;**35**:37-47
- [52] Pieczonka J, Piestrzyński A, Mucha J, Gluszek A, Kotarba M, Więclaw D. The red-bed type precious metal deposit in the Sieroszowice-Polkowice copper mining district. SW Poland. *Annales Societatis Geologorum Poloniae*. 2008;**78**:151-280
- [53] Pieczonka J, Piestrzyński A. Gold and other precious metals in copper deposit, Lubin, Sieroszowice district, SW Poland: Gold in Poland. *AM Monogra*. 2011;**2**:135-152
- [54] Bodine MW Jr. Trioctahedral clay mineral assemblages in Paleozoic marine evaporite rocks. In: Schreiber BC, Harner HL, editors. *Proceedings of the Sixth International Symposium on*
- Salt, Alexandria, Virginia, USA: Salt Institute: 1983 – Vol 1. Alexandria, Virginia, USA: Salt Institute; 1983: 267-284
- [55] Hryniv S, Peryt TM. Strontium distribution and celestite occurrence in Zechstein (Upper Permian) anhydrites of West Poland. *Chemie der Erde*. 2010; **70**:137-147
- [56] Karnkowski PH. Origin and evolution of the Polish Rotliegend Basin. *Polish Geological Institute Special Papers, Warszawa*. 1999;**3**:1-95